Overview of radiation induced point defects in silica-based optical fibers

Sylvain Girard[a,*], Antonino Alessi[a], Nicolas Richard[b], Layla Martin-Samos[c], Vincenzo De Michele[a,d], Luigi Giacomazzi[e], Simonpietro Agnello[d], Diego Di Francesca[f], Adriana Morana[a], Blaž Winkler[e], Imène Reghioua[a], Philippe Paillet[b], Marco Cannas[d], Thierry Robin[g], Aziz Boukenter[a], Youcef Ouerdane[a]

[a] Univ Lyon, UJM-Saint-Etienne, CNRS, Graduate School Optics Institute, Laboratoire Hubert Curien UMR 5516, Saint-Etienne F-42023, France
[b] CEA, DAM, DIF, Arpajon F-91297, France
[c] CNR-IOM/Democritos National Simulation Center, Istituto Officina dei Materiali, c/o SISSA, Trieste IT-34136, Italy
[d] Università degli Studi di Palermo, Dipartimento di Fisica e Chimica, Palermo I-90123, Italy
[e] Materials Research Laboratory, University of Nova Gorica, Vipavska 11c, Ajdovscina SI-5270, Slovenia
[f] CERN, CH-1211 Geneva 23, Switzerland
[g] iXblue Photonics, Lannion, F-22300, Lannion, France

A B S T R A C T

Silica-based optical fibers, fiber-based devices and optical fiber sensors are today integrated in a variety of harsh environments associated with radiation constraints. Under irradiation, the macroscopic properties of the optical fibers are modified through three main basic mechanisms: the radiation induced attenuation, the radiation induced emission and the radiation induced refractive index change. Depending on the fiber profile of use, these phenomena differently contribute to the degradation of the fiber performances and then have to be either mitigated for radiation tolerant systems or exploited to design radiation detectors and dosimeters. Considering the strong impact of radiation on key applications such as data transfer or sensing in space, fusion and fission-related facilities or high energy physics facilities, since 1970's numerous experimental and theoretical studies have been conducted to identify the microscopic origins of these changes. The observed degradation can be explained through the generation by ionization or displacement damages of point defects in the differently doped amorphous glass (SiO_2) of the fiber's core and cladding layers. Indeed, the fiber chemical composition (dopants/concentrations) and elaboration processes play an important role. Consequently, identifying the nature, the properties and the generation and bleaching mechanisms of these point defects is mandatory in order to imagine ways to control the fiber radiation behaviors. In this review paper, the responses of the main classes of silica-based optical fibers are presented: radiation tolerant pure-silica core or fluorine doped optical fibers, germanosilicate optical fibers and radiation sensitive phosphosilicate and aluminosilicate optical fibers. Our current knowledge about the nature and optical properties of the point defects related to silica and these main dopants is presented. The efficiency of the known defects to reproduce the transient and steady state radiation induced attenuation between 300 nm and 2 μm wavelength range is discussed. The main parameters, related to the fibers themselves or extrinsic - harsh environments, profile of use - affecting the concentration, growth and decay kinetics of those defects are also reviewed. Finally, the main remaining challenges are discussed, including the increasing needs for accurate and multi-physics modeling tools.

1. Introduction

Silica-based optical fibers are used for a large variety of applications ranging from high speed, high bandwidth data communications [1], diagnostics to point or distributed temperature or strain sensing [2]. Most of these applications exploit their low

---

attenuation that typically ranges below one dB km^{-1} at infrared (IR) telecom wavelengths. All the fiber intrinsic advantages explain that they are today widely used in telecommunications, structural health monitoring, the oil and gas industries and in medicine [3]. A very particular application case concerns their integration in harsh environments associated with ionizing or non-ionizing radiations as those encountered in space, high energy physics facilities, fusion and fission-related facilities [4,5]. Radiation usually strongly alters the functionality of commercial microelectronic technologies, preventing as a general rule, their use for dose levels exceeding a few Gy [6]. The optical fibers are generally used as part of data links for signal transport from the irradiation zones to instrumentation zone, free of radiations [7], later as key component of diagnostics [8,9] and today they serve as the sensitive element of numerous sensors' architectures, either punctual (Fiber Bragg Grating (FBG) [10]) or distributed technologies based on Rayleigh, Brillouin or Raman scattering [3].

It has been shown since more than 50 years that radiation degrades the fiber optical properties in a very complex way, the main change being called radiation induced attenuation (RIA). RIA corresponds to a decrease of the fiber transmission capability [4,11]. The RIA levels and kinetics strongly differ from one fiber to another [12]. Numerous studies have been devoted to the analysis of the underlying parameters driving this phenomenon, especially to develop more radiation tolerant devices. To understand the RIA origins, the basic mechanisms of the radiation effects at the molecular scale have to be studied. Nowadays, it's well established that point defects are created by either ionization or displacement damage processes leading to structural modifications in the pure or doped amorphous host silica matrix of both fiber core and cladding [13–15]. These radiation induced point defects are associated with optical absorption (OA) bands causing the observed excess loss under irradiation. Numerous experimental spectroscopic studies have been devoted to the characterization of the structure, optical or electronic properties of these point defects in silica as well as to the understanding of their thermal or photo-stabilities. The identification and attribution of these active centers, to a given molecular organization/configuration, is based on their specific signature responses which can be highlighted by using several crossing techniques such as the spectroscopic ones (absorption, luminescence, Raman, electron paramagnetic resonance…). A number of review papers [15–18], volumes and book chapters [19–21] as well as PhD thesis [22–25] have been devoted to the analysis of these optically-active point defects, mainly focusing on pure silica and Ge-doped silica. Even if a large part of these studies is of fundamental interest to understand the optical fiber responses, the fiber case notably differs from the one of bulk glass. Indeed, a fiber is manufactured by the successive deposition of numerous differently doped silica layers. Each of these layers will present a different radiation response, leading to a non-homogenous generation of defects in the optical fiber transverse cross-section. In addition to this composition inhomogeneity, the fibers are characterized by different internal stress levels in the various layers and at their interfaces, this stress being related to their manufacturing and drawing process. This stress will also affect the generation efficiencies of some of the defects, this is the case for example of the non-bridging oxygen hole centers (Si-NBOHC) that are more easily created from strained Si-O-Si bonds than from regular ones [26]. Furthermore, in optical fibers, the light can only be guided through guided modes that are in limited number, the relative light power associated to the mode propagating into each layer depends on the waveguide properties and so the contribution of the defects to the global RIA. For single-mode (SM) fibers, at Telecom wavelengths such as 1550 nm, between 15% and 40% of the light can be guided in the claddings of some specialty optical fibers. Under the modeling point of view, guiding properties, as a function of the fiber geometry, can be obtained by numerically solving Maxwell Equations [27,28] using experimentally determined macroscopic dielectric constants. However, the main theoretical efforts have been and are still mainly focused on the assignment between experimental spectroscopic signatures and point defects atomic structures [29,30], including attempts to understand generation and conversion mechanisms [29,31–34].

In this review, we focus the analysis on the fiber radiation response in the 300 nm–2000 nm spectral domain, discussing which are the main defects responsible for the fiber degradation when exposed to transient irradiations (*fusion facilities, military applications*) or steady state ones (*fission, high energy physics facilities*). Even if the active optical fibers such as the Erbium, Erbium-Ytterbium-doped ones are not directly discussed, it is today well-established that their radiation responses is explained by the host glass matrix selected for their incorporation that usually contains phosphorus and/or aluminum dopants (see [5] for more details).

2. Radiation effects on optical fibers

In this section, we briefly describe the radiation effects on optical fibers and their impact on the related applications, more details can be found in the recent review [4]. Three major effects are observed that can impact the functionality of fiber-based technologies:

- The radiation induced attenuation (RIA)
- The radiation induced emission (RIE)
- The radiation induced refractive index change (RIRIC)

The relative importance of these three phenomena depends on the considered fiber, the harsh environment and the fiber profile of use. RIA almost affects all targeted applications, RIE can generally be mitigated for most of the applications/environments. RIE can also be used for dosimetry purposes, exploiting the Cerenkov emission [35] or the radioluminescence [36]. RIRIC or compaction is mainly observed under neutron exposure [37,38] and will especially affect the performances of fiber-based sensors exploiting the glass structure to monitor environmental parameters and in-core instrumentation, exposed to very high fluences of fast neutrons, above 10^{19} n.cm^{-2} and to high doses of associated gamma radiations (GGy levels) [39,40].
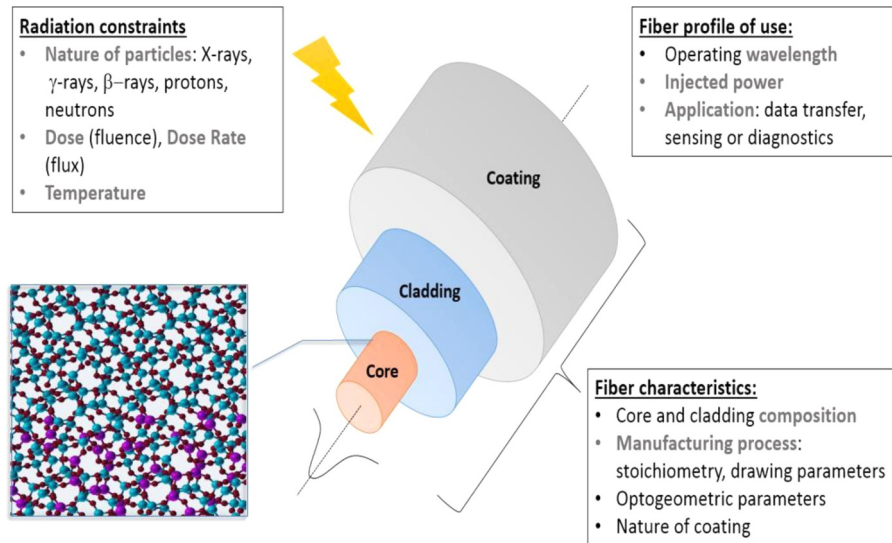
Fig. 1. Main parameters affecting the radiation response of a silica-based optical fiber in terms of RIA, RIE and RIRIC. The fiber structure is illustrated as well as the nature of the glass at the core and cladding interface. The inset illustrates a typical silica model used for ab initio calculation of the point defect properties: core is made of Ge-doped silica and the cladding is in pure silica (Si atoms are in red, Oxygen ones in green and Ge atoms in purple). (For interpretation of the references to colour in this figure legend, the reader is referred to the web version of this article.)

2.1. Radiation-induced attenuation

RIA corresponds to an increase of the fiber attenuation when exposed to radiation. RIA levels and kinetics depend on many parameters that are reviewed in Fig. 1 and explain why this research domain is still strongly active. Indeed, the response of a given silica-based fiber has been shown to depend on the irradiation characteristics: dose or fluence (expressed in Gy(SiO$_2$)) [12,41], the dose rate or flux (Gy(SiO$_2$/s)) [42,43], the temperature of irradiation [44,45] and of its profile of use: injected light power [46], operating wavelength [47,48]. Furthermore, the RIA levels strongly depend on the fiber intrinsic characteristics such as the composition of its core and cladding [4,49,50], its manufacturing process [51–53], its opto-geometric parameters [54] and its light guiding properties [55].

During the irradiation of the fiber at room temperature (RT), a RIA growth is usually observed and when the irradiation stops, for most of the fibers, the RIA decreases partially, reaching a permanent value depending strongly on the temperature. This behavior can be explained by competitive defect generation and bleaching mechanisms occurring during irradiation, while bleaching mechanisms clearly dominate the post-irradiation processes. The main parameter controlling the fiber radiation response in terms of RIA is its core and cladding composition. Usually, the fiber doping profiles are optimized to achieve two main objectives: first one is the design of the fiber refractive-index profile that defines the guided modes, confinement factor or sensing properties as its Brillouin signature. The second one is to ensure that the glass presents very low attenuation, reducing the absorption and Rayleigh scattering levels close to their theoretical limits.

For these reasons, the common doping elements (named dopants or codopants) are quite limited in number for passive optical fibers: germanium (Ge), fluorine (F), boron (B), phosphorus (P), aluminum (Al) and nitrogen (N). Most of the telecom-grade optical fibers possess a Ge-doped core and either a pure silica cladding or a cladding doped with a combination between the Ge, P and F dopants. Phosphorus and Aluminum dopants are widely used in the core of active optical fibers to reduce the clustering of the rare-earth ions (Er^{3+}, Yb^{3+}…) [56] and then improve the performances of the fiber-based amplifiers or lasers. As it was shown that fibers containing one of these two dopants are very radiation sensitive, the response of passive Al- and P-doped optical fibers is today more and more studied pushed by the increasing need for distributed dosimetry techniques. Boron is also today widely used in polarization-maintaining optical fibers or to increase the photosensitivity of germanosilicate optical fibers for easier FBG writing. No recent study has been really devoted to the impact of this dopant on the fiber radiation vulnerability. There exists another class of optical fibers, less studied in the literature, that have their cores doped with nitrogen through the reduced-pressure plasma chemical vapor deposition (SPCVD) process [57]. These N-doped fibers present several very interesting properties, including a good radiation tolerance at low doses for both transient [50] and steady state irradiations [50,57–59]. These fibers also present strong radioluminescence and optically stimulated luminescence that can serve for online monitoring of photon or proton beams [60]. Another class of fibers is not covered by this review, the microstructured and photonic band gap (PBG) fibers as only a few papers deal with their radiation response [61–65]. For the PBG fibers, these fibers present very low RIA levels under steady state γ-ray irradiation thanks to their air-core and pure silica structure [63,64]; for high dose rate transient exposures their potential sounds promising in comparison with usual PSC fibers but needs more investigations as an unusual dose dependence of the RIA was observed in [65].

Fig. 2 illustrates the RIA dose dependence at 1550 nm observed for four different optical fibers during a steady state X-ray irradiation: The pure-silica core (PSC) F-doped cladding optical fiber and Ge-doped, P-doped and Al-doped fibers, all with pure silica
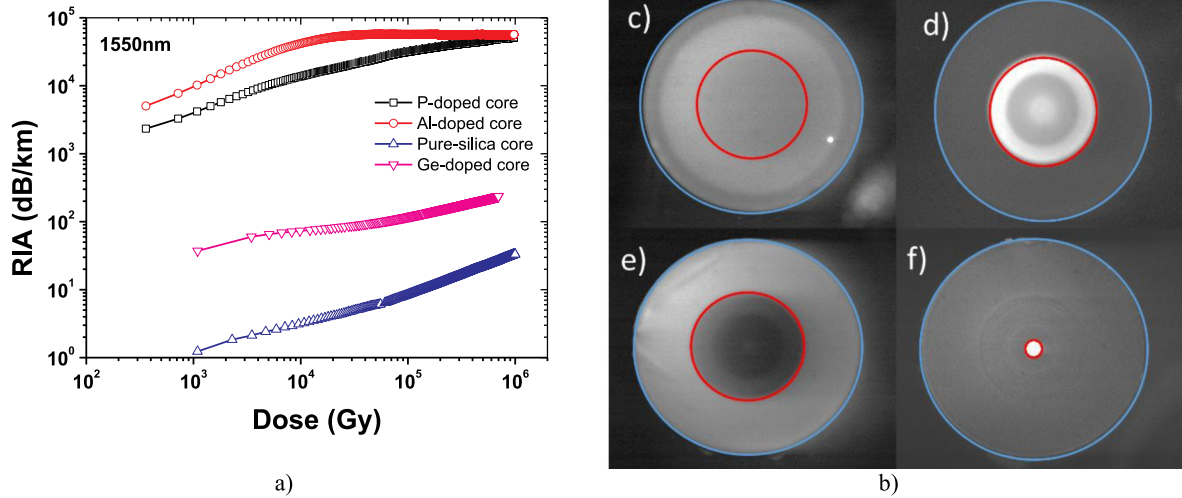
Fig. 2. a) Illustration of the X-ray RIA dose dependence measured at 1550 nm at RT for four different fibers: pure-silica core (PSC), Ge-, P- and Al-doped cores b) Cathodoluminescence panchromatic images of the fiber cross sections under ~ 20 keV electron beam: c) PSC fiber with luminescence bands peaking at 450 nm, 540 nm and 650 nm from defects present in both its core (red circle) and cladding (blue circle); d) Ge-doped MMF with defects emitting around 400 nm located in its core e) P-doped MMF without luminescence in its core; f) Al-doped SMF fiber with a strong core luminescence around 350 nm. The last three fibers present the same emitting centers in their claddings than the PSC fiber.(For interpretation of the references to colour in this figure legend, the reader is referred to the web version of this article.)

claddings. From this figure, it is evident that at 1550 nm, the third telecommunication window, the four fibers present very different vulnerabilities. The PSC fiber presents the lowest level of induced losses at this wavelength, with RIA of about ~ 40 dB.km^{-1} after 1 MGy dose. Indeed PSC fibers, together with F-doped fibers, have been shown to be the most radiation hardened waveguides for applications having to operate at such high dose levels: ITER [8,66], nuclear waste repository [67], nuclear industry [68] or high energy physics facilities [69,70]… In this case, their radiation response is even more complex as the RIA levels and kinetics are strongly influenced by the amounts of impurities (chlorine, hydroxyl groups) [71–74] and by the glass properties: fictive temperature [75], stoichiometry [76,77]. By affecting the glass structure and disorder, variation of the fiber manufacturing or drawing processes changes its radiation sensitivity by modifying the nature and concentration of the sites acting as precursor reservoir for the generation of the optically active radiation-induced defects: strained bonds, oxygen-deficient centers, oxygen-excess centers.

Hydrogen also plays a key role in the defect creation and bleaching mechanisms and then in defining the fiber vulnerability [78,79]. Indeed, hydrogen, coming either from the harsh environments [67] or generated by radiations through interaction with the fiber coating or cable material [38] is able to easily diffuse into the optical fibers with kinetics depending mainly on the temperature and fiber geometric parameters [80]. After reaching the fiber core, hydrogen interacts with the radiation-induced defects passivating some of them (see [80] for a detailed study). As a consequence, hydrogen loading was investigated for the radiation hardening of optical fibers, showing promising results mainly for pure-silica core in the visible-near infrared [8,81] and active Er- and ErYb-doped optical fibers at the pump and signal wavelengths [82,83]. This hardening technique is of no practical use if the loaded fibers are coated with polymers as H_2 will be able to diffuse out the fiber in a few weeks at room temperature. For long term operation of loaded fibers, dedicated structures, such as metal-coated optical fibers [84] or carbon-coated optical fibers were first suggested to ensure that hydrogen remains inside the fiber over long periods [83] but imply performing the loading treatment at both high pressure and high temperature (>300 °C). More sophisticated fiber structure has then been proposed, allowing to replenish the H_2 reservoir *in situ* during the irradiation at high doses thanks to the addition of longitudinal holes made in the fiber cladding [85]. Later this concept was combined with the implementation of a carbon coating, which allowed manufacturing H_2-loaded holey active fibers in an H_2 impermeable coating without employing too high pressure and temperature that can degrade their amplification properties (so called hole-assisted carbon-coated optical fibers) [86]. It must be pointed out that the passivation of the radiation induced point defects by hydrogen (or by deuterium, D_2) is accompanied by the generation of Si-OH (Si-OD) and Si-H (Si-D) bonds, resulting in increasing absorption at infrared wavelengths [80]. As a consequence, H_2 (or D_2) loading is not useful for applications needing optical fibers operating in the second or third telecom windows. For such cases, radiation hardening techniques are now focusing on the optimization of the preform fabrication regimes [76,77] as well as fiber drawing regimes [87].

Together with pure-silica core fibers (F-doped cladding), F-doped fibers are considered as the most radiation tolerant to high dose (>100 kGy) steady state γ-ray or X-ray irradiations and are used for a variety of applications in such environments from data links [69,70] to diagnostics [8,88].

However this class of fibers sounds less tolerant to transient high dose rate exposures, with very high transient loss levels [50] that prevent their use without appropriate treatments [89], e.g. by low dose pulsed pre-irradiation [90]. The Ge-doped fiber presents intermediate response with about ~ 250 dB.km^{-1} at the same dose level. This class of fibers can be used in radiation environments but only at low dose levels (<100 kGy), for relatively short lengths, the main application for such fibers under radiation are data links

and distributed sensing. Germanosilicate fibers are also widely used for FBG manufacturing as this glass is photosensitive but under radiation the use of FBGs written by femtosecond laser in pure or F-doped silica should be preferred to reduce the FBG degradation [10, 91]. Al and P-doped fibers are very radiation sensitive, having losses at 1.55 μm higher than 50000 dB/km at 1 MGy. These fibers cannot be used in radiation environments except to serve as radiation detectors or dosimeters [92–94]. The exceptional potential of P-doped fibers for dosimetry was first investigated in [95] and is today exploited in the various facilities of CERN for distributed 1D dose mapping thanks to its unique response at 1550 nm related to the generation of the P_1 defect [96,97].

2.2. The radiation-induced emission

When exposed to radiation, light can be generated into the optical fiber core and guided to the detection system. The RIE can originate from different mechanisms. For high flux of sufficiently energetic particles Cerenkov light is observed, only during the irradiation run. This Cerenkov signature is, for example, observed in the case of the optical fibers used for in-core monitoring [35] or for fibers used for plasma or laser diagnostics during an ignition shot and tested under very high dose rate pulsed X-rays [4]. In addition to Cerenkov, precursors or radiation induced defects can also be associated with luminescence bands and this signal can be observed during irradiation too. The RIE phenomenon is illustrated in Fig. 2b, that gives the panchromatic images recorded during cathodoluminescence measurements, i-e irradiation of the fiber cross section with 20 keV electrons and recording the generated luminescence (integrated between 300–800 nm) in the various fiber regions. As it can be easily seen by considering that all fiber claddings are made with the same pure silica, Ge and Al doping are associated with strong RIE while in case of P-doping, the RIE levels are strongly decreased. A complete characterization of the cathodoluminescence responses of the fiber types can be found in [98,99]. Today the RIE and luminescence properties of irradiated fiber-based materials are widely studied for dosimetry applications, particularly for medicine applications (see [100] for a recent review). The radioluminescence of Ge, Ce, Cu, N and Gd-doped glasses or of O_2 loaded pure-silica fibers are investigated for photons [36,101–103], protons [104,105] or neutrons [106] *in situ* beam monitoring. For passive dosimetry, the thermoluminescence properties of the Ge-doped fibers are also deeply characterized for post-irradiation ionizing and non-ionizing dose measurements [107,108], these fiber materials show performances overcoming those of commercially-available thermoluminescent dosimeters.

2.3. The radiation-induced refractive-index change

Radiation can change the glass structure, leading to a pure or doped silica compaction and refractive index (RI) changes. These effects are of primary importance when the fiber is used as a point or distributed sensor relying on the glass response to temperature or strain. The RIA leads to RI change via the Kramers-Kronig relations. Two main contributions are usually considered: the first one is related directly to absorption bands of point defects; the second one is related to densification, which can be estimated via the Lorentz-Lorenz relation [10,109–113]. Regarding the Lorentz-Lorenz relation, it was shown that i) the refractive index linearly increases with the density at a rate of ~ 0.18 g^{-1} cm^3 [13,109], ii) the densification ($\Delta\rho/\rho$) can be described by the law A $\times$ D^k, where A is a constant, D is the dose, and k is equal to 1 for fast neutrons and swift ions whereas it is on average 2/3 for γ-rays, electrons, or UV light [110,114] and iii) radiation induced densification is limited to 3–4% for pure silica [13,40,114]. On the other side, in the Kramers-Kronig relation the RIRIC increases with the amplitude of the induced absorption and it is inversely proportional to (λ^2-ζ^2), where λ is the wavelength at which the RIRIC has to be evaluated and ζ is the wavelength of the absorption [10]. Regarding the point defect contribution to RIRIC, it should be remembered that the concentrations of most of these defects tend to saturate at values lower than 10^{19} cm^{-3} for doses of ~ 10 kGy [13,115,116], exceptions being the SiE´ and NBOHC defects whose larger concentrations do not exceed 10^{20} cm^{-3}. As a consequence, the part of the RIRIC in the near-IR due to these UV absorbing defects can hardly be the sole responsible for the large RI variations reported at high doses or fluences. Obviously, for the low dose RIRIC the two contributions should be considered. On this regard, we note that the Kramers-Kronig relation usually employed remains an approximation [111] and that its correct evaluation requires the knowledge of the RIA spectral dependence in a large domain. In general, it seems possible to evaluate the contribution of a specific defect to the RIRIC, but it appears much more complicated to infer if one or more species of color centers are the unique origin of the RIRIC. Furthermore, in optical fibers different layers have different compositions and can be subjected to different starting stresses so that structural modification and defect generation can have spatial distributions. These spatial distributions can imply a spatial distribution of the RIRIC that can modify the guiding properties fixed by the refractive index profile.

3. Points defects related to SiO_2 and its main dopants

To make the transition between a phenomenological and trial-and-error based development model and a guided rational design of specialty fibers, a deep knowledge on the atomic structure and related spectroscopic signature of point defects is a basic requirement. In addition, clear maps of their formation and conversion mechanisms have to be drawn. Experimentally, it is desirable to have access to preforms and fibers that are manufactured *ad hoc* to have a sufficient knowledge and control on their chemical composition and manufacturing conditions. To distinguish such samples with commercially available ones, they are sometimes labeled with the prefix "canonical" in our studies (see [117–119] for more details). The main and standard characterization techniques comprise EPR, optical absorption (IR, visible and UV) and luminescence. In special cases, also Raman might provide with some insights [120–122]. In order to identify centers together with their corresponding generation and conversion mechanisms, it is necessary to monitor, analyze and compare the behaviors of several fiber samples when exposed to different radiation sources (photons, electrons, protons, neutrons…) and doses at different conditions as, for instance, temperature, pressure or loading with gases (H_2, O_2) [123–125].
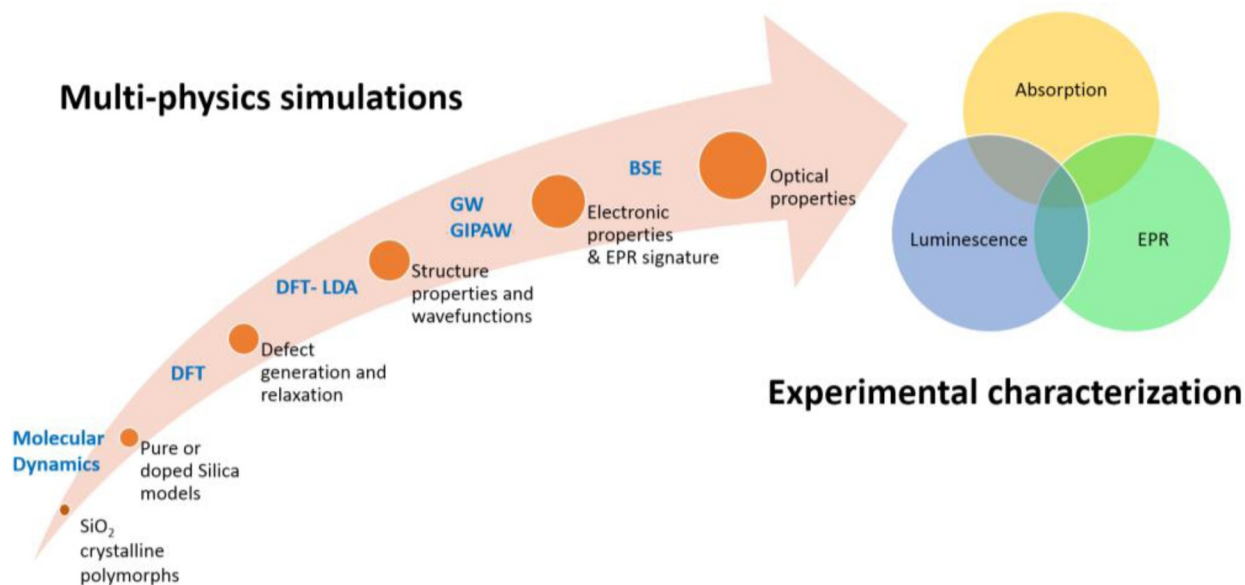
Fig. 3. Illustration of the coupled experimental /simulation approach used to identify the structural and optical properties of radiation-induced point defects in silica. More details can be found in [117–119].

Correlating some of the spectroscopic signatures and behavior to given center structures is, therefore, an expensive, formidable and cumbersome task which does not guarantee the construction of a meaningful model for the underlying atomic-scale mechanisms. In this context, atomic scale theoretical modeling might be a very useful complementary tool. Theoretically, electronic and optical properties of defects were historically (and sometimes still) addressed within the framework of Density Functional Theory (time dependent or not), (TD)-DFT, or Hartree-Fock and Configuration Interaction in very small cluster models or molecular analogs [33,34,126–128], in embedded clusters [129,130] or in bulks [131–137]. After the precursory work of E. Chang et al. [138] that demonstrated the accuracy of solving the Bethe-Salpeter Equation (BSE) within the GW approximation for modeling optical properties, the combination of both has become a standard in the field, that has allowed for univocal assignments between measured experimental optical bands and atomic structure [29,139]. Indeed, the BSE accounts, in a computationally efficient way, for screening and electron-hole interactions from first-principles. The development of the GIPAW [140–142] formalism based on DFT has represented also a revolution in the field that has opened the way for a parameter-free calculation of the EPR parameters as Fermi contacts and g-tensors. The GIPAW has successfully been applied to relate measured EPR parameters with the underlying atomic structure [143–146]. Fig. 3 describes at a glance the standards in modeling and spectroscopic characterization tools.

In this section, we review the main point defects reported in the literature in either the non-irradiated or irradiated glasses used to manufacture the silica-based optical fibers. For the classification, we considered first the defects observed in pure or F-doped silica glasses as fluorine has never been associated to a particular defect structure apart from Si-F linkage. However, its presence modifies the glass disorder resulting in lowering the concentrations of strain bonds and then the ones of some silica intrinsic defects [17]. Then, we review the point defects associated with the following dopants: Ge, P, Al. For each known defect, the following information are given if available: its structure, its paramagnetic or diamagnetic nature (allowing or not its EPR investigation), its associated OA band(s) (peak energy and full-width at half maximum (FWHM), oscillator strength), its optical luminescence (OL) band(s), if any (peak energy, FWHM, lifetime) as well as some of the key references about this particular defect structure. Latest available theoretical spectroscopic signatures are provided as references or explicitly discussed in the tables listing those properties.
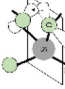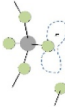
3.1. Point defects in pure silica

Table 1 reviews the main properties of the silica-related point defects identified in the literature on the basis of spectroscopic investigations: OA; OL or EPR combined with treatments such as irradiation, thermal annealing or gas loading (H_2, O_2 or D_2). It should be noticed that all defects cannot be characterized through the three techniques. As examples, the diamagnetic defects cannot be probed by EPR and only parts of the defects are luminescent centers. These experimental limitations combined together with the strong overlapping in the defect OA responses explain that these centers have been studied for the last 50 years. Today, part of these limitations can be overcome thanks to the development of new multi-physics simulation approach illustrated in Fig. 3.

To highlight the complexity of the RIA in the PSC optical fibers, Fig. 4 compares the RIA observed at RT in a MM PSC solarization-resistant optical fiber one second after an X-ray pulse (200 Gy(SiO_2) and dose rate > 1 MGy/s) [177] and during a continuous γ-ray irradiation at a dose of 200 Gy (3 mGy/s).

In both cases the higher RIA levels are observed in the visible domain with reduced degradation in the near-IR. For the transient X-ray pulsed irradiated fiber, no OA band can be distinguished in the RIA spectrum. The set of Gaussians used to fit the RIA spectra is

Table 1
Review of the main optical properties of pure-silica related point defects and those related to chlorine and hydrogen impurities.

Name	Structure	Param	OA peak eV (FWHM eV)	Oscillator strength	Note	PL, peak eV (FWHM eV, lifetime RT)	Refs
Oxygen deficient center ODC(II)	>Si:	No	5.05 (0.32)	0.15	S_0-S_1 transition ISC assisted (T_1-S_0 transition) S_0-T_1 transition	4.4 (0.4 eV; 4.0 ns) 2.75 (0.34; 10 ms) 2.75(0.34; 10 ms)	[16,29,156–159]
ODC(I)	≡Si-Si≡	No	3.15 (0.30)① 6.9 (0.4)	1.60 10^{-7} 0.1–0.2	PL features similar bands	4.4 and 2.7	[16,139,157,159–162]
Non-Bridging Oxygen Hole Centers NBOHC	≡Si-O•	Yes	7.6 (0.5–06) 1.97 (0.17) 4,8 (1.0) 6.4 (1.7)①	0.1–0.2 1.90 10^{-4} 0.05 0.05	Asymmetric Pekarian-shaped 5 Gaussian are needed to describe the absorption in UV VUV see ref [167] for the relative intensity	1.91 (0.17, 10–20 µs)	[16,121,163–169]
E'	≡Si•	Yes	5.8 (0.7)	0.1–0.2	Inherent	Not observed	[16,156,170–172]
Self-trapped hole STH$_1$		Yes	2.61 (1.2) 1,88 (0.2–0.5)	0.283②	Inherent Strain-assisted (observed in OF)	None reported None reported	[173–180] [173,177,178]
STH$_2$		Yes	2.16 (0.3–0.6) 1.63 (0.3–0.7)	0.283②	Inherent Strain-assisted (observed in OF)	None reported None reported	[173–180] [173,177,178]
Peroxy Linkage POL	Si-O-O-Si	No	3.8(0.2), 4.2(0.6, 7.3(0.2), 7.5(0.1)	~0.0005–0.003	Computational	None reported	[30]
Peroxy Radical POR	Si-O-O•	Yes	2.02, 4.08, 5.02 2.0, 4.8	0.00056, 0.052,0.035 0.0004, 0.2	Computational (one SiO$_4$ H-passivated tetrahedron cluster) experiment	–	[126,132,181]
Self-trapped Electron STE			3.7 4.6 6.4	– – –	Computational Computational Computational	– – –	[173,182] [173,182] [173,182]
Self-trapped Exciton STEX		No	4.2 (1.16) 5.3 (0.78)	– –	Computational Experimental	2.85 eV (theory) 2.6 −2.8 eV (exp)	Theory [183] Exp [184–189]
Ozone O$_3$	O$_3$	Yes	4.8 (0.8–0.86)	Cross section 1.2 10^{-17} cm^2	VUV UV bleaching can induce the O$_2$ emission [21]		[190,191]
O2	molecular oxygen	Yes	0.97 (0.013) 1.62 (0.013)	1.1 10^{-8} 4.2 10^{-9}	T1-S0 transition T1-S1 transition	0.97 (0.01 eV, 0.4–0.8 s)③	[192–198]
ClO	ClO	Yes	3.26 3.65	– –	– –	–	[88,177,199,200]
Cl^2	Cl^2	No	3.78 (0.6) 2.3	3.8 cross section 2.58 10^{-19} cm^2	Vibronic progression T<110 K	1.2 (0.42, 5 ms at 13 K)	[122]
H(I)	>Si'-H	Yes	Not observed	–	–	Not observed	[14,17,23]
LTRIA	STH	Yes	0.6 – 0.7 eV (non-Gaussian)	–	LTRIA is attributed to inherent STHs	Not observed	[153]

① Peak and FWHM derived from PLE spectra.
② Linear combination Gaussian bands peaking at 2.16 and 2.60 eV.
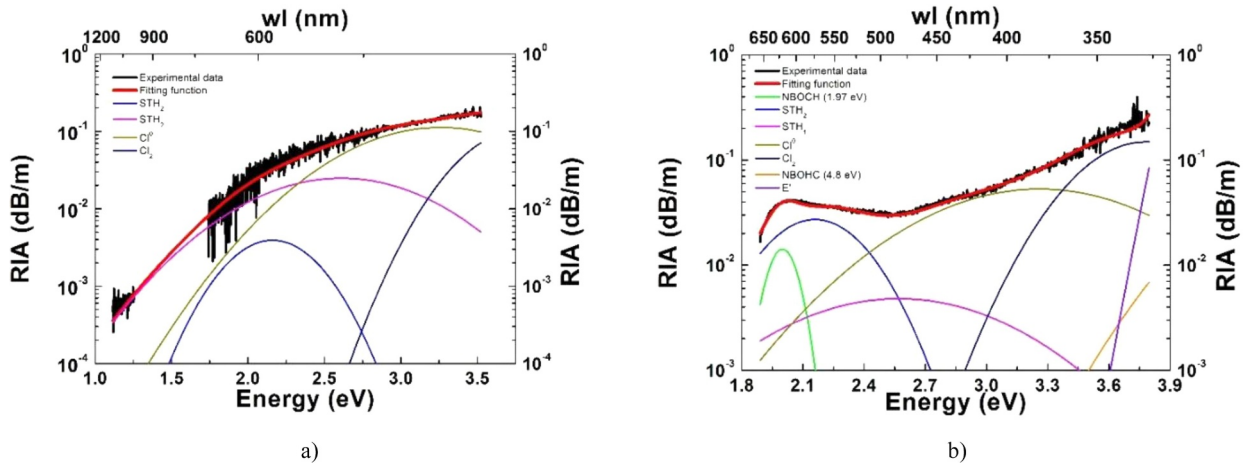③ Strong radioluminescence signal under X-rays [103].

Fig. 4. Illustration of the RIA spectra measured in a PSC solarization resistant multimode optical fiber (MMF) a) 1 s after an X-ray pulse at RT b) during γ-ray irradiation at 200 Gy (RT) with a dose rate of 3 mGy/s. The best achievable fits are reported using the set of defects described in Table 1 and the OA bands of the defects involved in the fiber response.

based on the data of Table 1 that reviews the main characteristics of the silica-related defects. It is evident that the most of the RIA above 2.5 eV is attributable to chlorine related defects such as Cl_2 and Cl^0. The defects absorbing too far in the UV such as ODC(I), E′ centers have no or negligible impact in the spectral range of interest for optical fibers. Similarly, the self-trapped holes (STHs), having life-time of the order of tens of seconds [12], represent the most absorbing defect for energies lower than 2.2 eV. The largest difference between the transient and continuous irradiations concerns the relative STH_1 and STH_2 amplitudes, highlighting the metastable nature of these defects. Furthermore, in the X-ray pulsed irradiated optical fibers, the contribution of NBOHC to the RIA was found to be negligible. In [74], the Gaussian deconvolution of the RIA spectra for times between ~0.2 and 1 s after X-ray pulse reveals that the RIA spectrum is well described by the two RIA bands due to strain-assisted STHs (1.66 eV and 1.83 eV). In a very recent work [147], it was found out that at smaller post-pulse times (~10 μs – 10 ms), the RIA decay occurs at much higher rate than at larger times. This supports the assumption that at shorter times the RIA can be explained by the contribution of the inherent STHs and their OA bands centered below 1 eV in the near-IR range. Theoretically, STHs in pure silica models have been addressed in the framework of DFT [148] and their formation at strained bonds discussed [149,150]. Still a large amount of work should be done to provide exploitable results in the context of fibers, especially as it was shown that the STHs' properties could differ between bulk and fibers.
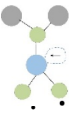
For environments associated with MGy dose levels, it was shown that by reducing the amount of Cl impurity, the contribution of the absorption bands of the Cl-related species to the UV and visible RIA can be minimized, the NBOHCs then becoming the main RIA contributor. This can be achieved in silica at the cost of increasing the hydroxyl groups (Si-OH) content ("wet" fibers) and by particular preform deposition technique allowing manufacturing optical fibers with both low-OH and low-Cl contents. This last category usually presents radiation response dominated by the STH contribution. To further improve the resistance of this class of fibers in the visible, it is possible to apply some pre-treatments such as H_2 loading before the radiation exposure. This hardening technique was first proposed by Nagasawa et al. [79] for optical fibers, its effects being later investigated in details for the ITER project [8,78,81] or for space applications (see Section 2.1).

For applications working in the IR domain, e.g. at the two 1310 and 1550 nm telecommunication wavelengths, it has been recently shown that O_2-loaded fibers exhibit better radiation-response than their classical counterparts, in particular the contribution of self-trapped holes defects to the IR-RIA seems lowered [76,77]. At larger doses (> 10 kGy) and in the IR domain, one long-wavelength non-Gaussian OA band peaking at the wavelength of >1.7 μm has also been observed in PSC fibers (as well as in Ge- and N-doped fibers) by several researchers [49,58,76,151,152]. The behavior of this absorption is very similar to that of low-temperature infrared absorption (LTIRA) discovered by Chernov et al. [153] that is associated with inherent STHs: both bands are peaking around 0.6–0.7 eV, are non-Gaussian and seem composed of a continuum of states. However, if the LTIRA component features very short lifetime [153], the former band appears very stable even at increased temperatures. As an example, this long-wavelength OA band stretch up to 1 μm at GGy doses and high neutron fluences associated with in-core testing and appears as the major RIA contributor at 1550 nm [151,152]. With regards to its thermal stability, this absorption may be different from the LTRIA one; for sure further studies are needed to improve our knowledge on the RIA origin in this spectral domain. A few studies [154,177,155] also report the possible presence of an OA band around 1 eV, observed today in PSC fibers which needs also further investigations to be definitively associated to a defect structure.

3.2. Germanium-related point defects

Table 2 reviews the main properties of the Ge-related point defects that were first discussed in the literature on the basis of OA, OL or EPR measurements and more recently through *ab initio* calculations. The properties of some of these defects have been deeply

Table 2
Germanium-related point defects: main optical characteristics and key references.

Name	Structure	Param	OA peak eV (FWHM eV)	Oscillator Strength	Note	PL peak eV (FWHM eV, lifetime RT)	Refs
GLPC	>Ge:	No	5.15 (0.41–0.46) / 3.8[④] / 7–8[④]	0.07–0.12 / 10^{-3} less intense	Direct $S_0{\to}S_1$ / ISC assisted / Direct $S_0{\to}T_1$ / Direct $S_0{\to}S_2$	4.3 (0.44;2 ns) / 3.2 (0.42; 110 µs) / 3.2 (0.42;110 µs) / 4.3 (0.44;2 ns) / 3.2 (0.42; 110 µs)	[21, 29,53,156,209,206]
Ge(1)	>Ġe<	Yes	4.4–4.5 (1–1.4; 1.97 in [179])	0.15–0.42 (0.28 in [179])	–	None reported	[179,206,210–212]
Ge-E'	≡Ge•	Yes	5.7–5.8 (1.2–1.5) / 6.2–6.3 (0.8–1.1)	0.4 in [211] / 0.7 (± 0.2 [211])	– / –	None reported / None reported	[111,210,211] / [18,206,211]
Ge(2)	>Ġe< or >Ge or	Yes	5.8 (0.9–0.74)	0.6–0.77 (in 0.5 [179])	–	None reported	[179,206, 212,213]
GeX[④]	?	?	2.61 (0.97)		–	None reported	[206]
Ge-NBOHC	≡Ge-O•	Yes	2.1–1.89[④]	?	UV and VUV bands	1.86–1.84 (0.16–1.18;5 µs)	[214]
		Yes	3.68[④]	?	should be expected as for NBOHC		[214]
H(II)	>Ġe-H	Yes	from 4 up 5.5 in [215]	see ref [215]	–	None reported	[215]
?	?	?	2.54[④]	–?	–	1.83 (not reported) [④]	[216]
?	?	?	composite 4.9–2.5[④]	–	?	1.82 (not reported) [④]	[217]
?	?	?	4–2.5[④]	–	?	1.82 (0.4[④], 60 ns)	[218]
GeY	?	?	1.38 (0.71)	–	?	None reported	[219]
Transient defect	?	?	3.26 (1.4)	–	The existence has been proposed after X-ray pulsed irradiation	None reported	[205]
Ge-STH	?	Yes	0.54 (0.35)	–	The existence of Ge related self-trapped hole should be investigated	None reported	[49]

[①] Excitation of the PL.
[②] FWHM should be obtained by fit of the composite spectrum, lifetime not measured.
[③] need further studies.
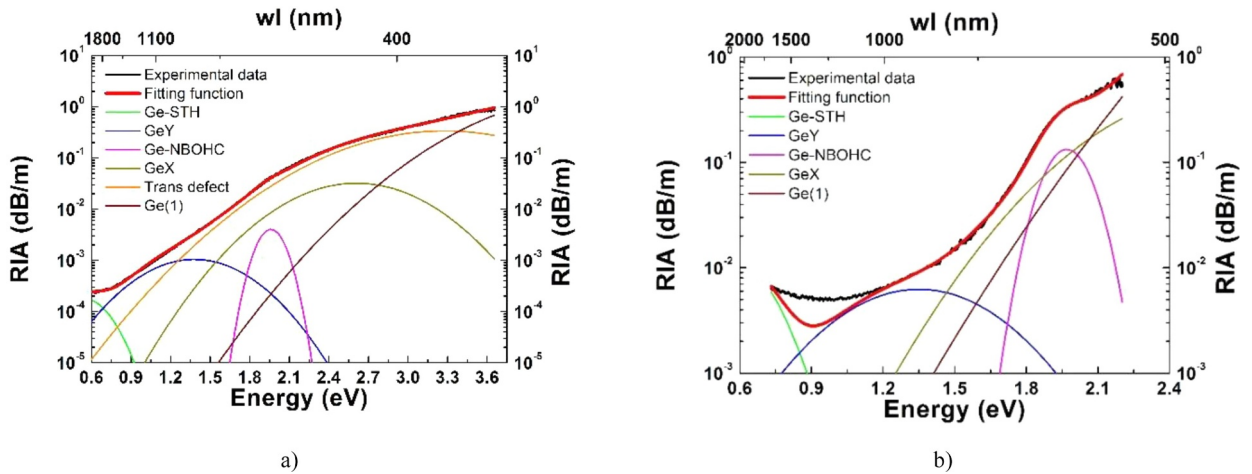[④] should extracted from OA fit or PLE.

Fig. 5. Illustration of the RIA spectra measured in a Ge-doped MMF a) 1 s after an X-ray pulse at room temperature (RT, 200 Gy, > 1MGy/s) b) during γ-ray irradiation at 200 Gy (RT) at 4 mGy/s. The best achievable fits are reported using the set of defects described in Table 2 and the corresponding OA bands.

studied such as the ones of the GeE′, Ge(1), and Ge(2) defects as they can be easily investigated in bulk or preform samples [179,201]. Other defects, only impacting at larger wavelengths (typically above 400 nm) have been less characterized even if they strongly affect the Ge-doped fiber transmission properties in the visible – near-IR, this is for example the case of GeX defects whose structure is still unknown.

Fig. 5a) illustrates the RIA spectra measured one second after an X-ray pulse (200 Gy(SiO$_2$), dose rate > 1 MGy/s) for a Ge-doped multimode fiber (62.5 μm core diameter; undoped cladding) [202]. Fig. 5b) shows the RIA spectra measured under steady state γ-rays after the same dose (~4mGy/s) in the same fiber. Both tests were done at RT and the comparison between the obtained results highlights the existence and contribution of metastable defects, which strongly contribute to RIA at high dose rate or low temperature irradiations. These unstable defects cannot easily be studied by *post mortem* analysis such as EPR measurements. These results are typical of the ones obtained for Ge-doped SMFs or MMFs. The choice to study a MMF rather than a SMF is explained by the fact that the influence of the light guiding effects on the IR-RIA spectra is minimized in large core fibers. The RIA levels are larger in the UV and visible ranges than in the IR and no OA bands can be easily distinguished as a result of the overlapping between the numerous bands of Ge-related defects. These two RIA spectra were reproduced using the set of defects reported in Tables 1 and 2. A first important result is that in the case of Ge-doping of the silica glass the generation of Ge-related defects is favored compared to the Si-related ones. The latter centers are present but contribute less to the induced losses in the visible-IR spectral as discussed on the basis of *ab initio* calculations [139].

Before discussing the RIA spectra, it must be pointed out that the OA and OL signatures of some of these defects such as Germanium Lone Pair Centers (GLPC) or the Ge-Non Bridging Oxygen Hole Centers (Ge-NBOHCs) are observed in both non-irradiated germano-silicate preforms and optical fibers [203,204]. GLPCs that are present in the native fibers serve as precursor sites for the generation of Ge (1) and Ge(2) defects under irradiation [115,125]. As a consequence, the GLPC concentration decreases with the dose [59] explaining their absence in the RIA spectra. As shown in Fig. 5 defects such as Ge-E′ or Ge(2) absorbing in the UV part of the spectrum can only marginally contribute to the RIA in the 400 nm – 2000 nm spectral range where germanosilicate optical fibers are used. Indeed, at lower wavelengths, their linear attenuation is too high even before irradiation for signal transmission. In the visible range, Ge(1), GeX and Ge-NBOHC defects mainly explained the observed RIA during steady state X-rays, γ-rays or neutron exposures [205–208].

For the case of transient exposures, as those associated with ignition experiments, the contribution of a RT metastable defect absorbing around 3.28 eV [205] appears as mandatory to reproduce the RIA spectra (see Fig. 5a. orange band). It is interesting to consider that adding this defect allows to fully reproduce the transient IR-RIA spectra. This defect seems absent under steady-state γ-ray irradiation but for this case, the RIA spectral dependence in the near-IR cannot be explained by the defect set reported in Table 2. Regarding the contributing defects, if the nature and properties of Ge(1) and Ge-NBOHC have been deeply studied, the GeX properties remain mostly unknown despite its practical importance for visible, near-IR applications. In the near-IR, the origins of the RIA in the germanosilicate optical fibers are still unknown. Very recently, an OA band around 900 nm (1.38 eV) has been observed and associated to a Ge-related defect, named as GeY. Its structure is still unknown. At larger wavelengths, this long wavelength RIA has been tentatively explained by the generation of Ge-STHs by analogy with the work of Chernov in pure silica [153], but further studies are needed to confirm this hypothesis (see Section 3.1 for a more detailed discussion). Ge-STHs and GeY defects are still not sufficient to reproduce the measured RIA, at least another source of optical losses around 0.9 eV has to be identified for continuous irradiation. For transient ones, the transient band at 3.28 eV in combination with them allows to fully reproduce the RIA spectrum. It must also be pointed out that the concentrations and properties of these Ge-defects can be affected by the presence of other codopants such as P or F in fibers with mixed composition. Finally, in Table 2 the emission properties of these defects are also reported as they can be exploited for a variety of dosimetry-related applications.

Table 3

Phosphorus-related point defects: main optical characteristics and key references.

Name	Structure	Param	OA peak eV (FWHM) eV	Oscillator strength	Note	PL peak eV (FWHM eV, lifetime RT)	Refs
m-POHC[①]		Yes	2.2 (0,35)	0.5		None reported	[116,220,222]
			2.5 (0,63)	0.5		None reported	
			5.3 (0,74)	0.5		None reported	
s-POHC[①]			3.1 (0,73)	0.5		None reported	[116,220,222]
P1		Yes	0.79 (0,29)	0.0007		None reported	[116,220, 222]
P2		Yes	4.5 (1,27)	0.035		None reported	[116,220, 222]
P4		Yes	4.8 (0,41)	0.014		None reported	[116,220, 222]
PO2		No	> 5.5 eV	Unknown	Unknown	None reported	[223]
P_2O_3[②]		No	5.9[③]	0.001		None reported	[224]
$[(O-)_3-P:]^0$ [224]			6.1[③]	0.05		None reported	[224]
			6.4[③]	0.04		None reported	[224]
Type I PODC [225]			8	0.3	Small cluster simulation	None reported	[225]
			8.43	0.2	Small cluster simulation	None reported	[225]
PO_2[②]		No	4.7 (0,7) [④]	0.002		3 (highly asymmetric; 5–6 ms)	[226]
			6.4 (0,6) [④]	comparable with the 4.7 PLE peak		3 (highly asymmetric; 5–6 ms)	
P2O5[②]		No	6.9[③]	0.004–0.006		None reported	[224]
$[(O-)_3-P = O]^0$			7.16[③]	0.002		None reported	[224]
[224]			7.2[③]	0.002		None reported	[224]
PO3**		No	6.1[③]	0.009		None reported	[224]
			6.5[③]	0.006		None reported	[224]
$[(O-)_2-P(=O)_2]^0$			7.2[③]	0.009		None reported	[224]
[224]			5.1–5.4[③]	0.001		None reported	[224]
PODC II		No	6.82–6.99	0.02–0.1	Small cluster simulation	None reported	[225]

[①] POHC EPR intensity correlates to the sum of all the OA bands.
[②] in ref [220].
[③] from ab-initio simulation.
[④] from PL excitation.

3.3. Phosphorus-related point defects

Table 3 reviews the main properties of the P-related point defects. If this dopant is associated with a variety of absorbing centers, only one luminescence band around 400 nm has been attributed to a P-related species. A very complete and pioneer work basing on OA and ESR measurements on thermally-treated and irradiated samples was published by D.L. Griscom in 1983 [220], recent deep theoretical and experimental investigations of the radiation effects in phosphosilicate glasses have been done by L. Giacomazzi et al. [224] and D. Di Francesca et al. [116] respectively. As phosphosilicate glasses are more transparent in the UV (before irradiation) than Ge-doped optical fibers, these fibers could be adapted for some specific applications in the 300 nm–2 μm domain. As an example, P-doped fibers have been designed for the laser diagnostics of megajoule class lasers [205,221]. Fig. 6 compares the RIA spectra measured for a P-doped MMF after an X-ray pulse and during a steady state irradiation (here with 40 keV X-ray instead of γ-rays). Once again, the obtained spectra have been fitted using the set of P-defects reported in Table 3. For both irradiation cases, these fibers are shown to be very radiation sensitive with loss levels as high as 100 dB m^{-1} at 600 nm after a 200 Gy dose.
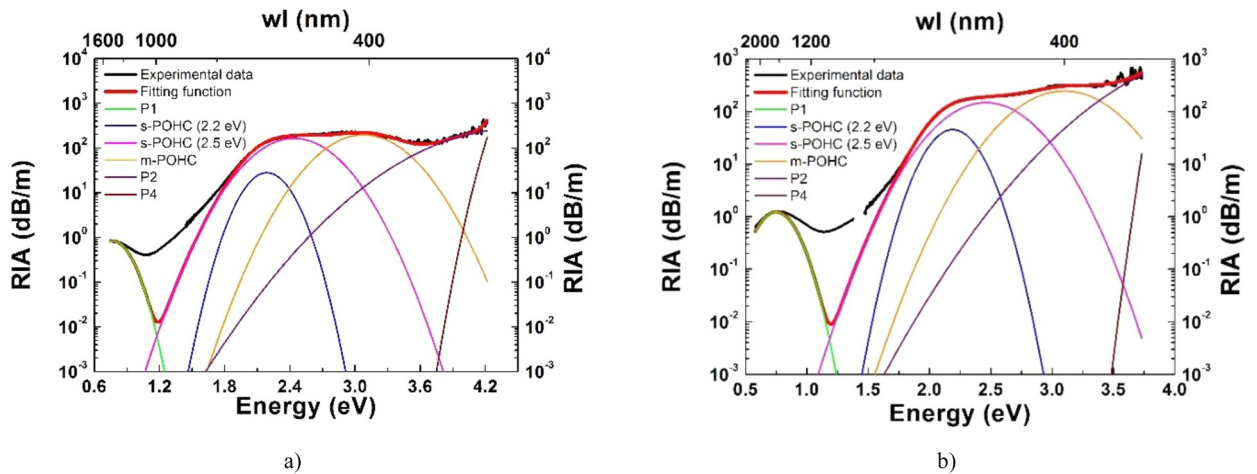
Fig. 6. Illustration of the RIA spectra measured in a P-doped MMF a) 10 s after an X-ray pulse at room temperature (RT, 200 Gy, > 1MGy/s) b) during X-ray irradiation at 200 Gy (RT) at 100 mGy/s. The best achievable fits are reported using the set of defects described in Table 3 and the corresponding OA bands.

In the visible and near-IR range, the induced losses are mainly caused by the OA band of the various forms (stable, metastable as defined by [220]) of the phosphorous-oxygen hole centers (POHC) with small contributions from the P_2 and P_4 OA bands absorbing at wavelengths below ~ 400 nm (E > 3 eV). At infrared wavelengths, the OA band of P_1 defect can be easily distinguished but this single defect cannot explain all the losses in this spectral domain. Our analysis clearly highlights that we still miss the origin of the RIA around 1.2 eV. It should be noted that adding a new OA band (free peak position and FWHM) seems not sufficient to reproduce the RIA spectra.

Indeed, at least two additional components seem needed. These phosphosilicate glasses are well adapted to dosimetry applications as well as a host matrix for active optical fibers. Hardening studies on Er and Er-Yb fiber amplifiers show that the P-related defects, especially P_1-centers, can be efficiently bleached by the hydrogen-loading of the glass or by Ce-codoping [82,86]. Another particularity of this defect is that its concentration can increase after the end of the irradiation, as it was shown that POHCs can recombine into P_1 at room temperature [220].

3.4. Aluminum-related point defects

Literature devoted to Al-related point defects remains significantly less well supplied than for the other silica-associated centers. First results have been obtained for natural silica that contains Al as impurity [227–229], only in few cases the investigated samples have Al contents that can be compared to those used for optical fiber manufacturing [55,230–232]. As a consequence, whereas for the natural silica it is accepted that the Al can be inserted in the glass matrix replacing the Si and with an alkaline charge compensator as neighbor [228,229] in doped silica (some weight percent) this aspect still needs further investigations to be confirmed. Table 4 details the optical absorption bands associated with the Al-defects. As shown in Fig. 7, this defect set is sufficient to describe the RIA measured in the UV–visible spectral range in aluminosilicate fibers both during X-ray steady state irradiation and a few seconds after a pulsed X-ray. Regarding these attributions we notice that the relation between the Al-OHC and the 2.3 eV OA band is well supported by various investigations [232,228], whereas the others have still to be confirmed. As an example, there are some investigations in which the 2.3 eV OA band is clearly present in the RIA spectrum whereas the 3.2 eV seems absent or with a smaller relative amplitude [228] with respect to those observed in [232,230]. Anyway, the bands reported in Table 4 are not sufficient to fit the data from the UV to the NIR as evidenced in [230]. Recent investigations have highlighted that the Al-doped fibers are good candidates for radiation detection [55], a better understanding of the Al insertion in silica matrix as well as the properties of its related defects represents, for sure, one of the future challenges.

4. Conclusion

In this review paper, we presented the main macroscopic radiation effects on optical fibers: the radiation induced attenuation, the radiation induced emission and the radiation-induced refractive index change. The amplitudes and kinetics of these changes depend on a large number of parameters, some of them being related to the fibers such as composition or manufacturing processes; others are extrinsic such as the ones related to the irradiation characteristics and the fiber profile of use. These macroscopic effects can mainly be explained by the point defects generated by radiation in the pure or doped silica layers constituting the fiber core and cladding. Understanding their generation and bleaching mechanisms, identifying their optical properties (absorption, luminescence) and thermal stabilities allow devising ways to control the fiber radiation response. Such optimization is done to enhance the fiber radiation resistance, hardening studies, as it was successfully proved by the H_2 loading treatments of the fibers or by the codoping of

Table 4

Aluminum-related point defects: main optical characteristics and key references.

Name	Structure	Param.	OA peak eV (FWHM eV)	Oscillator strength	Note	PL peak eV (FWHM eV, lifetime RT)	Refs
Al-OHC	≡Al-Ȯ-Si≡	Yes	2.3 (0.9)	0.060	PL excited in the range 1.7–2.5	1.5–1.0 and 0.7–0.2	[232,233]
			3.2 (1)	0.124	Proposed by simulation	Unknown	
			4.9 (1.08)	0.126	See ref [233] for the oscil. strength	Unknown	
AlE′	≡Al•	Yes	4.1(1.02)	0.214		Unknown	[232]
			4.9 (1.08)	0.126		Unknown	
?	?	?	Higher than 7.5 eV	Unknown	Structureless induced absorption under ArF irradiation at 80 K	Unknown	[228]
Transit ODC(II)	?	No ?	Excitation ArF laser	Unknown	The decrease of the 2.7 Pl was attributed to the back relaxation	4–4.5 (not reported; 4.5 ns)	[228]
Modified				Unknown	of the surrounding	2.7 (not reported,1.7 ms)[①]	

[①] afterglow during hundreds of seconds after switching off the laser [228]; recombination between STHS and modified ODCs(II).
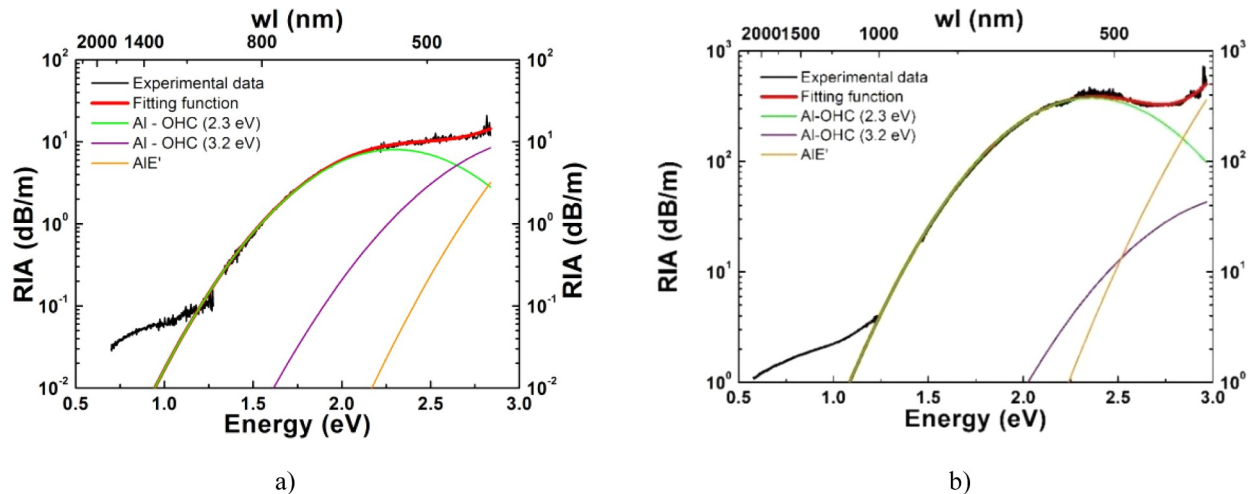

Fig. 7. Illustration of the RIA spectra measured in an Al-doped MMF a) 1 s after a pulsed X-ray (6.2 Gy, > 1MGy/s) b) during X-ray irradiation at 200 Gy (RT) at 100 mGy/s. The best achievable fits are reported using the set of defects described in Table 4 and the contributing OA bands.

P or Al-doped fibers with Ce^{3+} ions. There is also today an increasing interest for using radiation sensitive optical fibers for radiation detection or dosimetry. In this paper, we presented typical responses of the four main types of fibers to both pulsed X-ray irradiations (representative of fusion by inertial confinement constraints) and steady state X-ray or γ-rays irradiation (representative of space and nuclear industry constraints). We reviewed the today's knowledge about the point defects related to silica, Ge, P and Al and discussed how the known defects can explain the measured RIA. Though the identified defects are usually able to reproduce the loss excess in the UV and visible, for most of the fiber types, it is clearly shown that we are still missing part of the infrared RIA origins despite the large use of fibers at Telecom wavelengths. Historically most of the acquired knowledge was obtained by combining various experimental spectroscopic techniques such as absorption, luminescence, or electron paramagnetic resonance. Today with the establishment of very accurate and parameter free first-principle approaches, as GW-BSE and GIPAW, it becomes possible to somehow overcome the experimental limitations and to support the correlation between defect structure and experimentally observed signatures. However, the application of parameter-free accurate approaches, that overcome the known drawbacks of Density Functional based-frameworks, on complex models (interacting dopants and/or defects) larger than few hundreds of atoms, requires an order of magnitude leap in computational power to be achieved successfully. In addition, the accurate modeling of self-trapping through electronic excitations, as well as luminescence is yet not straightforward. Only one group was able to perform the extremely computationally demanding calculation of the structure and luminescence of Self-Trapped Excitons in quartz [183] within the GW-BSE framework. On the other side, while point defects in pure silica have attracted most of the theoretical efforts, primary, because of their interest for microelectronics, the number of available studies decreases significantly for Ge-doped silica and furthermore for other dopants relevant for optical fibers. Indeed, entire class of dopants, impurities and related defects lack, even, from an atomic-scale structure model that reproduce some experimental spectroscopic signatures and/or explain some measured behavior. The

drawing of an exhaustive map of defects and dopants together with their spectroscopic signature and generation and conversion mechanisms that links experimental results with atomic-scale models is a priority.

References

[1]   G.P. Agrawal, Fiber-Optic Communications Systems, 3rd ed., John Wiley & Sons, Inc, 2002.
[2]   D.A. Krohn, T.W. MacDougall, A. Mendez, Fiber Optic Sensors: Fundamentals and Applications, 4th ed., SPIE Press Book, 2015.
[3]   A.H. Hartog, An Introduction to Distributed Optical Fibre Sensors, 1st ed., CRC Press, 2018.
[4]   S. Girard, et al., Radiation effects on silica-based optical fibers: recent advances and future challenges, IEEE Trans. Nucl. Sci. 60 (2013) 2015.
[5]   S. Girard, et al., Recent advances in radiation-hardened fiber-based technologies for space applications, J. Opt. 20 (2018) # 093001.
[6]   M. Bagatin, S. Gerardin, Ionizing Radiation Effects in Electronics: From Memories to Imagers, 1st ed., CRC Press, 2015.
[7]   P.B. Lyons, et al., Fiber optic utilization at the Nevada Test Site, Report (1978) (digital.library.unt.edu/ark:/67531/metadc1203152/m1/1/: accessed January 7 (2019).
[8]   B. Brichard, et al., Radiation-hardening techniques of dedicated optical fibres used in plasma diagnostic systems in ITER, J. Nuc. Mat. 329–333 (2004) 1456.
[9]   J.L. Bourgade, et al., Present LMJ diagnostics developments integrating its harsh environment, Rev. Sci. Instr. 79 (2008) 10F301.
[10] A.I. Gusarov, S.K. Hoeffgen, Radiation effects on fiber gratings, IEEE Trans. Nucl. Sci. 60 (2013) 2037.
[11] E.J. Friebele, Overview of Radiation Effects in Fiber Optics 541 SPIE, 1985, p. 70 Vol.
[12] M. Van Uffelen, Modélisation de Systèmes D'acquisition Et De Transmission à Fibres Optiques Destinés à Fonctionner En Environnement Nucléaire, Thèse De Doctorat, Université de Paris XI, Paris, 2001.
[13] R.A.B. Devine, J-P. Duraud, E. Dooryhee, Structure and Imperfections in Amorphous and Crystalline Dioxide, Wiley, Chichester, U.K, 2000.
[14] April 8 - 20, 2000, Defects in SiO and Related Dielectrics, Science and technology: science and technology", in: G. Pacchioni, L. Skuja, D.L. Griscom (Eds.), proceedings of the NATO Advanced Study Institute on Defects in SiO$_2$ and Related Dielectrics: Science and Technology, Erice, Springer Science & Business Media, Italy, 2000April 8 - 20, 2000Eds.
[15] D.L. Griscom, Nature of Defects and Defect Generation in Optical Glasses 541 SPIE, 1985, p. 38 vol.
[16] L. Skuja, Optical properties of defects in silica, in: G. Pacchioni, L. Skuja, D.L. Griscom (Eds.), Defects in and Related Dielectrics: Science and Technology (NATO Science Series II), Kluwer, Dordrecht, The Netherlands, 2000, pp. 73–116.
[17] L. Skuja, M. Hirano, H. Hosono, K. Kajihara, Defects in oxide glasses, Phys. Stat. Sol. (c) 2 (2005) 15.
[18] V.B. Neustruev, Color centres in germanosilicate glass and optical fibres, J. Phys. Condens. Mater. 6 (1994) 6901.
[19] D.L. Griscom, The natures of point defects in amorphous silicon dioxide, in: G Pacchioni, L. Skuja (Eds.), Defects in SiO$_2$ and Related Dielectrics: Science and Technology, Kluwer Academic Publishers, Dordrecht, The Netherlands, 2000, pp. 117–159 Eds.
[20] D.L. Griscom, Intrinsic and extrinsic point defects in a-SiO$_2$, in: R.A.B. Devine (Ed.), The Physics and Technology of Amorphous, Plenum, New York, 1988, p. 125 Ed.
[21] M. Leone et al., Optical absorption, luminescence, and ESR spectral properties of point defects in silica, in silicon-based material and devices, (2001) 1.
[22] M. Cannas, Point defects in amorphous SiO$_2$: optical activity in the visible, UV and Vacuum-UV Spectral Regions, Università di Palermo, Palermo, Italy, 1998 Ph.D. dissertation.
[23] S. Agnello, Gamma Ray Induced Processes of Point Defect Conversion in Silica, Università di Palermo, Palermo, Italy, 2000 Ph.D. dissertation.
[24] G. Buscarino, Experimental Investigation on the Microscopic Structure of Intrinsic Paramagnetic Point Defects in Amorphous Silicon Dioxide, Università di Palermo, Palermo, Italy, 2007 Ph.D. dissertation.
[25] A. Alessi, Germanium Point Defects Induced by Irradiation in Ge-Doped Silica, Università di Palermo, Palermo, Italy, 2009 Ph.D. dissertation.
[26] R.A.B. Devine, J. Arndt, Defect pair creation through ultraviolet radiation in dense, amorphous SiO$_2$, Phys. Rev. B 42, 2617 (R) (1990).
[27] D. Marcuse, P. Liao, Theory of Dielectric Optical Waveguides, 2nd ed., Optics & Photonics Series, 2012.
[28] A.W. Snyder, J.D. Love, Optical Waveguide Theory, Chapman and Hall, 1983.
[29] L. Giacomazzi, et al., Photoactivated processes in optical fibers: generation and conversion mechanisms of twofold coordinated Si and Ge atoms, Nanotechnology 28 (2017) 195202.
[30] B. Winkler, et al., Correlations between structural and optical properties of peroxy bridges from first principles, J. Phys. Chem. C 121 (2017) 4002.
[31] Z. Chen, J. Wang, Y. Song, X. Zuo, First-principles investigation of oxygen-excess defects in amorphous silica, AIP Advances Adv. 7 (2017) 105118.
[32] T. Uchino, T. Yoko, Density functional theory of structural transformations of oxygen-deficient centers in amorphous silica during hole trapping: structure and formation mechanism of the E′γ center, Phys. Rev. B 74 (2006) 125203.
[33] T. Uchino, M. Takahashi, T. Yoko, Structure and generation mechanism of the peroxy-radical defect in amorphous silica, Phys. Rev. Lett. 86 (2001) 4560.
[34] T. Uchino, M. Takahashi, T. Yoko, Formation and decay mechanisms of electron–hole pairs in amorphous SiO$_2$, Appl. Phys. Lett. 80 (2002) 1147.
[35] B. Brichard, et al., Fibre-optic gamma-flux monitoring in a fission reactor by means of Cerenkov radiation, Meas. Sci. Technol. 18 (2007) 3257.
[36] A. Vedda, et al., Ce^{3+}-doped fibers for remote radiation dosimetry, Appl. Phys. Lett. 85 (2004) 6356.
[37] W. Primak, Fast-neutron-induced changes in quartz and vitreous silica, Phys. Rev. B 110 (1958) 1240.
[38] B. Brichard, et al., Radiation effect in silica optical fiber exposed to intense mixed neutron-gamma radiation field, IEEE Trans. Nucl. Sci. 48 (2001) 2069.
[39] L. Remy, et al., Compaction in optical fibres and fibre Bragg gratings under nuclear reactor high neutron and gamma fluence, IEEE Trans. Nucl. Sci. 63 (2016) 2317.
[40] G. Cheymol, et al., Study of fibre Bragg grating samples exposed to high fast-neutron fluences", IEEE Trans. Nucl. Sci. 65 (2018) 2494 9.
[41] D.L. Griscom, M.E. Gingerich, E.J. Friebele, Model for the dose, dose-rate and temperature dependence of radiation-induced loss in optical fibers, IEEE Trans. Nucl. Sci. 41 (1994) 523.
[42] H. Henschel, O. Köhn, H.U. Schmidt, Influence of dose rate on radiation induced loss in optical fibres, in Proc. 1399 SPIE, 1991, p. 49.
[43] E.J. Friebele, C.G. Askins, M.E. Gingerich, Effect of low dose rate irradiation on doped silica core optical fibers, Appl. Opt. 23 (1984) 4202 1984.
[44] A.T. Ramsey, W. Tighe, J. Bartolick, P.D. Morgan, Radiation effects on heated optical fibers, Rev. Sci. Instrum. 68 (1997) 632.
[45] S. Girard, et al., Combined high dose and temperature radiation effects on multimode silica-based optical fibers, IEEE Trans. Nucl. Sci. 60 (2013) 4305.
[46] H. Henschel, O. Kohn, Regeneration of irradiated optical fibres by photobleaching? IEEE Trans. Nucl. Sci. 47 (2000) 699.
[47] P. Borgermans, Spectral and Kinetic Analysis of Radiation Induced Optical Attenuation in Silica: Towards Intrinsic Fiber Optic Dosimetry? Thèse de doctorat, Vrije Universiteit, Brussels, 2001.
[48] O. Deparis, Etude Physique Et Expérimentale De La Tenue Des Fibres Optiques Aux Radiations Ionisantes Par Spectrométrie Visible-Infrarouge, Ph.D. dissertation, Faculté Polytechnique de Mons, Mons (1997).
[49] E. Regnier, et al., Low-dose radiation-induced attenuation at infrared wavelengths for P-doped Ge-doped and pure silica-core optical fibres, IEEE Trans. Nucl. Sci. 54 (2007) 1115.
[50] S. Girard, et al., Gamma-rays and pulsed X-ray radiation responses of nitrogen, germanium doped and pure silica core optical fibers, Nucl. Instrum. Methods Phys. Res. B 215 (2004) 187.
[51] B. Brichard, S. Agnello, L. Nuccio, L. Dusseau, Comparison between point defect generation by gamma-rays in bulk and fibre samples of high purity amorphous silica, IEEE Trans. Nucl. Sci. 55 (2008) 2121.
[52] S. Girard, et al., Transient radiation effects on optical fibers for megajoule class lasers: influence of MCVD process parameters, IEEE Trans. Nucl. Sci. 59 (2012) 2894.
[53] G. Origlio, et al., Influence of the drawing process on the defect generation in multistep-index germanium-doped optical fibers", Opt. Lett. 34 (2009) 2282.
[54] J. Kuhnehnn, H. Henschel, U. Weinand, Influence of coating material, cladding thickness, and core material on the radiation sensitivity of pure silica core step-

index fibers, presented at the 8th Eur. Conf. RADECS (2005) paper A2.

[55] G. Li Vecchi, et al., Infrared radiation induced attenuation of radiation sensitive optical fibers: influence of temperature and modal propagation", IEEE Trans. Nucl. Sci. (2018) under review.

[56] G. Vienne, et al., Role of aluminum in ytterbium-erbium codoped phosphoaluminosilicate optical fibers, Opt. Fiber Technol. 2 (1996) 387.

[57] E.M. Dianov, et al., Low-hydrogen silicon oxynitride optical fibers prepared by SPCVD, J. Lightw. Technol. 13 (1995) 1471.

[58] A.L. Tomashuk, et al., Performance of special radiation-hardened optical fibers intended for use in the telecom spectral windows at a megagray level, IEEE Trans. Nucl. Sci. 45 (1998) 1566.

[59] Diego Di Francesca, Roles of Dopants, Interstitial O_2 and Temperature in the Effects of Irradiation on Silica-based Optical Fibers, University of Saint-Étienne, Saint-Etienne, 2015 Ph.D. dissertation.

[60] S. Girard, et al., X-rays, γ-rays and proton beam monitoring with multimode nitrogen-doped optical fiber, IEEE Trans. Nucl. Sci. 66 (2019) 306.

[61] A.F. Kosolapov, et al., Optical losses in as prepared and gamma-irradiated microstructured silica-core optical fibers, Inorg. Mater. 40 (2004) 1229.

[62] S. Girard, et al., Transient radiation-induced effects on solid core microstructured optical fibers, Opt. Exp. 19 (2011) 21760.

[63] H. Henschel, J. Kuhnhenn, U. Weinand, High radiation hardness of a hollow core photonic band gap fiber," presented at the 8th Eur, Conf. RADECS, 05 2005 paper LN4.

[64] G. Cheymol, H. Long, J.F. Villard, B. Brichard, High level gamma and neutron irradiation of silica optical fibers in CEA OSIRIS nuclear reactor, IEEE Trans. Nucl. Sci. 55 (2008) 2252.

[65] S. Girard, J. Baggio, J.-L. Leray, Radiation-induced effects in a new class of optical waveguides: the air guiding photonic crystal fibers, IEEE Trans. Nucl. Sci. 52 (2005) 2683.

[66] T. Kakuta et al., Round-robin irradiation test of radiation resistant optical fibers for ITER diagnostic application, J. Nucl. Mater.307–311 (2202) 1277.

[67] S. Delepine-Lesoille, et al., France's state of the art distributed optical fibre sensors qualified for the monitoring of the French underground repository for high level and intermediate level long lived radioactive wastes, Sensors 17 (2017) 1377.

[68] A. Morana, et al., Influence of neutron and gamma-ray irradiations on rad-hard optical fiber, Opt. Mat. Exp. 5 (2015) 898.

[69] T. Wijnands, Radiation tolerant optical fibers: from sample testing to large series production, J. Lightw. Technol. 29 (2011) 3393.

[70] T. Wijnands, et al., Optical absorption in commercial single mode optical fibers in a high energy physics radiation field, IEEE Trans. Nucl. Sci. 55 (2008) 2216.

[71] L. Skuja and N. Ollier, Optical properties of chlorine- and oxygen-related defects in SiO2 glass and optical fibers, in advanced photonics2018, paper BM2A.1.

[72] S. Shibata, M. Nakahara, Fluorine and chlorine effects on radiation-induced loss for GeO_2-doped silica optical fibers, J. Lightw. Technol. 3 (1985) 860.

[73] K. Nagasawa, M. Tanabe, K. Yahagi, Gamma-ray-induced absorption bands in pure-silica-core fibers, Jpn. J. Appl. Phys. 23 (1984) 1608.

[74] S. Girard, D.L. Griscom, J. Baggio, B. Brichard, F. Berghmans, Transient optical absorption in pulsed-X-ray-irradiated pure-silica-core optical fibers: influence of self-trapped holes, J. Non-Cryst. Solids 352 (2006) 2637.

[75] B.H. Babu, et al., Radiation hardening of sol gel-derived silica fiber preforms through fictive temperature reduction, Appl. Opt. 20 (2016) 7455.

[76] A.L. Tomashuk, et al., Enhanced radiation resistance of silica optical fibers fabricated in high O_2 excess conditions, J. Lightw. Technol. 32 (2014) 213.

[77] P.F. Kashaikin, et al., Radiation-induced attenuation in silica optical fibers fabricated in high O_2 excess conditions, J. Lightw. Technol. 33 (2015) 1788.

[78] B. Brichard, Systèmes à Fibres Optiques Pour Infrastructures Nucléaires: du Durcissement Aux Radiations à l'application, Thèse de doctorat, IES—Institut d'Electronique du Sud, Montpellier (2008).

[79] K. Nagasawa, Y. Hoshi, Y. Ohki, K. Yahagi, Improvement of radiation resistance of pure silica core fibers by hydrogen treatment, Jpn. J. Appl. Phys. 24 (1985) 1224.

[80] J. Stone, Interactions of hydrogen and deuterium with silica optical fibers: a review, J. Lightw. Technol. 5 (1987) 712.

[81] B. Brichard, et al., Radiation-induced absorption spectra in H_2-soaked pure silica core fibres, J. Non-Cryst. Sol. 353 (2007) 466.

[82] S. Girard, et al., Radiation hardening techniques for Er/Yb doped optical fibers and amplifiers for space application, Opt. Express 20 (2012) 8457.

[83] K.V. Zotov, et al., Radiation-resistant erbium-doped fiber for spacecraft applications, IEEE Trans. Nucl. Sci. 55 (2008) 2213.

[84] A.L. Tomashuk, et al., Radiation-induced absorption and luminescence in specially hardened large-core silica optical fibers, IEEE Trans. Nucl. Sci. 47 (2000) 693.

[85] A.F. Kosolapov, S.L. Semjonov, A.L. Tomashuk, Improvement of radiation resistance of multimode silica-core holey fibers, Proc. SPIE 6193 (2006) 61931E.

[86] S. Girard, et al., Radiation-hard erbium optical fiber and fiber amplifier for both low and high dose space missions, Opt. Lett. 39 (2014) 2541.

[87] P.F. Kashaykin, et al. Influence of drawing conditions on radiation-induced attenuation of pure-silica-core fibers in the near-IR range, Proc. SPIE10681(2018) 1068110.

[88] S. Girard, C. Marcandella, Transient and steady state radiation responses of solarization-resistant optical fibers, IEEE Trans. Nucl. Sci. 57 (2010) 2049.

[89] A.L. Tomashuk, et al., Pulsed-bremsstrahlung-radiation effect on undoped- and Ge-doped-silica-core optical fibers at wavelength of 1.55 μm, J. Lightw. Technol. 35 (2017) 2143.

[90] A.L. Tomashuk, et al., Role of inherent radiation-induced self-trapped holes in pulsed-radiation effect on pure-silica-core optical fibers, J. Lightw. Technol. 37 (2019) 956.

[91] A. Morana, et al., Radiation tolerant fiber Bragg gratings for high temperature monitoring at MGy dose levels, Opt. Lett. 39 (2014) 5313.

[92] M.C. Paul, et al., Radiation response behavior of high phosphorous doped step-index multimode optical fibers under low dose gamma irradiation, J. Non-Cryst. Solids 355 (2009) 1496.

[93] S. Girard, et al., Feasibility of radiation dosimetry with phosphorus-doped optical fibers in the UV-visible range of wavelengths, J. Non-Cryst. Solids 357 (2011) 1871.

[94] A. Alessi, et al., Radiation effects on aluminosilicate optical fibers: spectral investigations from the ultraviolet to near-infrared domains, Phys. Status Solidi A (2018) 1800485.

[95] H. Henschel, O. Köhn, H.U. Schmidt, Optical fibres as radiation dosimeters, Nucl. Instrum. Meth. Phys. Res. B 69 (1992) 307.

[96] D. Di Francesca, et al., Distributed optical fiber radiation sensing in the proton synchrotron booster at CERN, IEEE Trans. Nucl. Sci. 65 (2018) 1639.

[97] D. Di Francesca, et al., Qualification and calibration of single mode phosphosilicate optical fiber for dosimetry at CERN, J. Lightw. Technol. (2019).

[98] I. Reghioua, et al., Cathodoluminescence characterization of point defects in optical fibers, IEEE Trans. Nucl. Sci. 64 (2017) 2318.

[99] I. Reghioua, Cathodoluminescence Characterization of Point Defects in Silica-Based Materials: Optical Fibers and Nanoparticles, Université de Saint-Etienne, France, 2018 PhD Thesis.

[100] S O'Keeffe, et al., A review of recent advances in optical fibre sensors for *in vivo* dosimetry during radiotherapy, Br. J. Radiol. 88 (2015) 20140702.

[101] N. Al Helou, et al., Effects of ionizing radiations on the optical properties of ionic copper-activated sol-gel silica glasses, Opt. Materials Mater. 75 (2018) 116.

[102] N. Al Helou, et al., Radioluminescence and optically stimulated luminescence responses of a cerium-doped sol-gel silica glass under X-ray beam irradiation, IEEE Trans. Nucl. Sci. 65 (2018) 1591.

[103] D. Di Francesca, Near infrared radio-luminescence of O_2 loaded Rad-Hard silica optical fibers: a candidate dosimeter for harsh environments, Appl. Phys. Lett. 105 (2014) 183508.

[104] S. Girard, et al., Potential of copper- and cerium-doped optical fiber materials for proton beam monitoring, IEEE Trans. Nucl. Sci. 64 (2017) 567.

[105] C. Hoehr, et al., Novel Gd^{3+}-doped optical fiber material for proton therapy dosimetry, Sci. Rep. (2019) submitted to.

[106] M. Dehnel, N. Savard, C. Penner, D. Potkins, C. Hoehr, Characteristics of a Ce-doped silica fiber irradiated by 0 - 400 MeV neutrons, IEEE Sensors 2018 Conference, New Delhi, October 2018, https://doi.org/10.1109/ICSENS.2018.8589510.

[107] Y.A. Abdulla, Y.M. Amin, D.A. Bradley, The thermoluminescence response of Ge-doped optical fibre subjected to photon irradiation, Rad. Phys Chem. 61 (2001) 409.

[108] M. Benabdesselam, et al., Performance of Ge-doped optical fiber as a thermoluminescent, IEEE Trans. Nucl. Sci. 60 (2013) 4251.

[109] R.A.B. Devine, Ion implantation- and radiation-induced structural modifications in amorphous SiO_2, J. Non-Cryst. Sol. 152 (1993) 50.

[110] R.E. Schenker, W.G. Oldham, Ultraviolet-induced densification in fused silica, J. Appl. Phys. 82 (1997) 1065.

[111] A. Alessi, et al., Refractive index change dependence on Ge(1) defects in γ-irradiated Ge-doped silica, Phys. Rev. B 80 (2009) 014103.

[112] D.C. Hutchings, M. Sheik-Bahae, D.J. Hagan, E.W. Van Stryland, Kramers-Krönig relations in nonlinear optics, Opt. Quant. Elect. 24 (1992) 1.

[113] R. Kitamura, L. Pilon, M. Jonasz, Optical constants of silica glass from extreme ultraviolet to far infrared at near room temperature, Appl. Opt. 46 (2007) 8118.

[114] G. Buscarino, S. Agnello, F.M. Gelardi, R. Boscaino, Polyamorphic transformation induced by electron irradiation in a-SiO_2 glass, Phys. Rev. B 80 (2009) 094202.

[115] A. Alessi, et al., Evolution of photo-induced defects in Ge-doped fiber/preform: influence of the drawing, Opt. Express 19 (2011) 11680.

[116] D. Di Francesca, et al., Combined temperature radiation effects and influence of drawing conditions on phosphorous doped optical fibers, Physica Status Solidi A (2018) 201800553.

[117] S. Girard, et al., Radiation effects on silica-based preforms and optical fibers - i: experimental study with canonical samples, IEEE Trans. Nucl. Sci. 55 (2008) 3743.

[118] S. Girard, et al., Radiation effects on silica-based preforms and optical fibers - II: coupling Ab initio simulations and experiments, IEEE Trans. Nucl. Sci. 55 (2008) 3508.

[119] N. Richard, et al., Coupled theoretical and experimental studies for the radiation hardening of silica-based optical fibers, IEEE Trans. Nucl. Sci. 61 (2014) 1819.

[120] A. Alessi, et al., Phosphorous doping and drawing effects on the Raman spectroscopic properties of O = P bond in silica-based fiber and preform, Opt. Mater. Express 2 (2012) 1391.

[121] D. Di Francesca, et al., Resonance Raman of oxygen dangling bonds in amorphous silicon dioxide, J. Raman Spectrosc. 48 (2016) 230.

[122] L. Skuja, et al., Luminescence and Raman detection of molecular Cl_2 and ClClO molecules in amorphous SiO_2 matrix, J. Phys. Chem. C 121 (2017) (2017) 5261.

[123] S. Girard, et al., On-site regeneration technique for hole-assisted optical fibers used in nuclear facilities, IEEE Trans. Nucl. Sci. 62 (2015) 2941.

[124] D. Di Francesca, et al., Influence of O_2 -loading pretreatment on the radiation response of pure and fluorine-doped silica-based optical fibers, IEEE Trans. Nucl. Sci. 61 (2014) 3302.

[125] D. Di Francesca, et al., O_2 loading treatment of Ge-doped silica fibers: a radiation hardening process, J. Lightw. Techn. 34 (2016) 2311.

[126] C. Sousa, C. de Graaf, Optical properties of peroxy radicals in silica: multiconfigurational perturbation theory calculations, J. Chem. Phys. 114 (2001) 6259.

[127] T. Uchino, Y. Kitagawa, T. Yoko, energies Structure, and vibrational properties of silica rings in SiO_2 glass, Phys. Rev. B 61 (2000) 234.

[128] A.H. Edwards, W.B. Fowler, Theory of the peroxy-radical defect in α-SiO_2. *Phys. Rev. B* **26** (192) 6649.

[129] P. V.Sushko, A.L. Shluger, C. Richard, A. Catlow, Relative energies of surface and defect states: ab initio calculations for the MgO (001) surface, Surf. Sci. 450 (2000) 153.

[130] L. Giordano, P.V. Sushko, G. Pacchioni, A.L. Shluger, Optical and EPR properties of point defects at a crystalline silica surface: ab initio embedded-cluster calculations, Phys. Rev. B 75 (2007) 024109.

[131] A. Stirling, A. Pasquarello, First-principles modeling of paramagnetic Si dangling-bond defects in amorphous SiO_2. *Phys. Rev. B* **66** (2002) 245201.

[132] D. Donadio, M. Bernasconi, M. Boero, Ab initio simulations of photoinduced interconversions of oxygen deficient centers in amorphous silica, Phys. Rev. Lett. 87 (2001) 195504.

[133] G. Roma, Y. Limoge, Density functional theory investigation of native defects in SiO_2: self-doping and contribution to ionic conductivity, Phys. Rev. B 70 (2004) 174101.

[134] L. Martin-Samos, et al., Neutral self-defects in a silica model: a first-principles study, Phys. Rev. B 71 (2005) 014116.

[135] Layla Martin-Samos, Yves Limoge, Guido Roma, Defects in amorphous SiO_2: valence alternation pair model, Phys. Rev. B 76 (2007) 104203.

[136] L. Giacomazzi, P. Umari, A. Pasquarello, Medium-range structure of vitreous SiO_2 obtained through first-principles investigation of vibrational spectra, Phys. Rev. B 79 (2009) 064202.

[137] M. Gerosa, et al., Communication: Hole localization in Al-doped quartz SiO_2 within ab initio hybrid-functional DFT, *J. Chem. Phys.* **143** (2015) 111103.

[138] E.K. Chang, M. Rohlfing, S.G. Louie, Excitons and optical properties of α-quartz, Phys. Rev. Lett. 85 (2000) 2613.

[139] N. Richard, et al., Oxygen deficient centers in silica: optical properties within many-body perturbation theory, J. Phys. Cond. Matter. 25 (2013) 335502.

[140] C.J. Pickard, F. Mauri, All-electron magnetic response with pseudopotentials: NMR chemical shifts, Phys. Rev. B 63 (2001) 245101.

[141] J.R. Yates, C.J. Pickard, F. Mauri, Calculation of NMR chemical shifts for extended systems using ultrasoft pseudopotentials, Phys. Rev. B 76 (2007) 024401.

[142] C.J. Pickard, F. Mauri, First-principles theory of the EPR g tensor in solids: defects in quartz, Phys. Rev. Lett. 88 (2002) 086403.

[143] G. Pfanner, C. Freysoldt, J. Neugebauer, U. Gerstmann, Ab initio EPR parameters for dangling-bond defect complexes in silicon: effect of Jahn-Teller distortion, Phys. Rev. B 85 (2012) 195202.

[144] Z. Zeng, C.S. Garoufalis, S. Baskoutas, G. Bester, Electronic and optical properties of ZnO quantum dots under hydrostatic pressure, Phys. Rev. B 87 (2013) 125302.

[145] L. Giacomazzi, et al., EPR parameters of E′ centers in v$-SiO_2$ from first-principles calculations, Phys. Rev. B 90 (2014) 014108.

[146] L. Giacomazzi, L. Martin-Samos, N. Richard, Paramagnetic centers in amorphous GeO_2, Microelectron. Eng. 147 (2015) 130.

[147] A.L. Tomashuk, et al., Role of inherent radiation-induced self-trapped holes in pulsed-radiation effect on pure-silica-core optical fibers, J. Lightw. Technol. 37 (2019) 956.

[148] A.V. Kimmel, P.V. Sushko, A.L. Shluger, Structure and spectroscopic properties of trapped holes in silica, J. Non-Cryst. Solids 353 (2007) 599.

[149] M. d'Avezac, M. Calandra, F. Mauri, Density functional theory description of hole-trapping in SiO_2: a self-interaction-corrected approach, Phys. Rev. B 71 (2005) 205210.

[150] M. Farnesi Camellone, T.D. Kühne, D. Passerone, Density functional theory study of self-trapped holes in disordered SiO_2, Phys. Rev. B 80 (2009) 033203.

[151] B. Brichard, et al., Radiation effect in silica optical fiber exposed to intense mixed neutron–gamma radiation field, IEEE Trans. Nucl, Sci. 48 (2001) 2069.

[152] G. Cheymol, et al., High level gamma and neutron irradiation of silica optical fibers in CEA OSIRIS nuclear reactor, IEEE Trans. Nucl, Sci. 55 (2008) 2252.

[153] P.V. Chernov, Spectroscopic manifestations of self-trapped holes in silica, Phys. Stat. Sol. 115 (1989) 663.

[154] S. Girard, et al., Transient radiation responses of optical fibers: influence of MCVD process parameters, IEEE Trans. Nucl. Sci. 59 (2012) 2894.

[155] P.F. Kashaykin, et al., Radiation induced attenuation in pure silica polarization maintaining fibers, J. Non-Cryst. Solids 508 (2019) 26.

[156] L. Skuja, Isoelectronic series of twofold coordinated Si, Ge, and Sn atoms in glassy SiO_2: a luminescence study, J. Non-Cryst. Solids 149 (1992) 77.

[157] H. Nishikawa, E. Watanabe, D. Ito, Y. Ohki, Decay kinetics of the 4.4-eV photoluminescence associated with the two states of oxygen-deficient-type defect in amorphous SiO_2, Phys. Rev. Lett. 72 (1994) 2101.

[158] R. Boscaino, M. Cannas, F.M. Gelardi, M. Leone, Spectral and kinetic properties of the 4.4-eV photoluminescence band in a-SiO_2: effects of γ irradiation, Phys. Rev. B 54 (1996) 6194.

[159] L. Skuja, Optically active oxygen-deficiency-related point defects in amorphous silicon dioxide, J. Non-Cryst. Solids 239 (1998) 16.

[160] H. Hosono, Y. Abe, H. Imagawa, H. Imai, K. Arai, Experimental evidence for the Si-Si bond model of the 7.6-eV band in SiO_2 glass, Phys. Rev. B 44 (1991) 12043.

[161] M. Cannas, et al., Absorption band at 7.6 eV induced by γ-irradiation in silica glasses, J. Non-Cryst. Solids 280 (2001) 188.

[162] S. Agnello, et al., Competitive relaxation processes of oxygen deficient centers in silica, Phys. Rev. B 67 (2003) 033202.

[163] L. Skuja, Point defects in silica glass: luminescence and optical absorption: the origin of the intrinsic 1.9 eV luminescence band in glassy SiO_2, J. Non-Cryst. Solids 179 (1994) 51.

[164] H. Hosono, et al., Vacuum ultraviolet optical absorption band of non-bridging oxygen hole centers in SiO_2, Solid State Commun. 122 (2002) 117.

[165] M. Cannas, F.M. Gelardi, Vacuum ultraviolet excitation of the 1.9-eV emission band related to nonbridging oxygen hole centers in silica, Phys. Rev. B 69 (2004) 153201.

[166] L. Vaccaro, M. Cannas, R. Boscaino, Luminescence features of nonbridging oxygen hole centres in silica probed by site-selective excitation with tunable laser, Solid State Commun. 146 (2008) 148.

[167] L. Skuja, K. Kajihara, M. Hirano, H. Hosono, Visible to vacuum-UV range optical absorption of oxygen dangling bonds in amorphous SiO_2, Phys. Rev. B 84 (2011) 205206.

[168] L. Skuja, M. Hirano, H. Hosono, Oxygen-related intrinsic defects in glassy SiO_2: interstitial ozone molecules, Phys. Rev. Lett. 84 (2000) 302.
[169] A. Morana, et al., Origin of the visible absorption in radiation-resistant optical fibers, Opt. Mater. Express 3 (2013) 1769.
[170] R. Boscaino, M. Cannas, F.M. Gelardi, M. Leone, ESR and PL centers induced by gamma rays in silica, Nucl. Instrum. Methods Phys. Res. B 116 (1996) 373.
[171] F. Messina, M Cannas, In situ observation of the generation and annealing kinetics of E' centres induced in amorphous SiO_2 by 4.7 eV laser irradiation, J. Phys. Condens. Matter 17 (2005) 3837.
[172] S. Agnello, G. Buscarino, F.M. Gelardi, R. Boscaino, Optical absorption band at 5.8 eV associated with the $E'\gamma$ centers in amorphous silicon dioxide: optical absorption and EPR measurements, Phys. Rev. B 77 (2008) 195206.
[173] P.F. Kashaykin, et al., Anomalies and peculiarities of radiation-induced light absorption in pure silica optical fibers at different temperatures, J. Appl. Phys. 121 (2017) 213104.
[174] D.L. Griscom, Self-trapped holes in amorphous silicon dioxide, Phys. Rev. B 40 (1989) 4224.
[175] D.L. Griscom, Electron spin resonance characterization of self-trapped holes in amorphous silicon dioxide, J. Non-Cryst. Solids 149 (1992) 137.
[176] M. Lancry, et al., EPR reversible signature of self-trapped holes in fictive temperature-treated silica glass, J. Appl. Phys. 123 (2018) 113101.
[177] V. De Michele, et al., Pulsed X-ray radiation responses of solarization-resistant optical fibers, Phys. Status Solidi A (2018) 201800487.
[178] Y. Sasajima, K. Tanimura, Optical transitions of self-trapped holes in amorphous SiO_2, Phys. Rev. B 68 (2003) 014204.
[179] David L. Griscom, On the natures of radiation-induced point defects in GeO_2-SiO_2 glasses: reevaluation of a 26-year-old ESR and optical data set, Opt. Mater. Express 1 (2011) 400.
[180] S. Girard, C. Marcandella, Transient and steady state radiation responses of solarization-resistant optical fibers, IEEE Trans. Nucl. Sci. 57 (2010) 2049.
[181] L. Skuja, K. Tanimura, N. Itoh, Correlation between the radiation induced intrinsic 4.8 eV optical absorption and 1.9 eV photoluminescence bands in glassy SiO_2, J. Appl. Phys. 80 (1996) 3518.
[182] A.-M. El-Sayed, M.B. Watkins, V.V. Afanas'ev, A.L. Shluger, Nature of intrinsic and extrinsic electron trapping in SiO_2, Phys. Rev. B 89 (2014) 125201.
[183] S. Ismail-Beigi, S.G. Louie, Self-trapped excitons in silicon dioxide: mechanism and properties, Phys. Rev. Lett. 95 (2005) 156401.
[184] W Hayes, et al., ODMR of recombination centres in crystalline quartz, J. Phys. C Solid State Phys. 17 (1984) 2943.
[185] S Guizard, P Martin, G Petite, P D'Oliveira, P Meynadier, Time-resolved study of laser-induced colour centres in SiO_2, J. Phys. Condens. Matter 8 (1996) 1281.
[186] K. Tanimura, T. Tanaka, N. Itoh, Creation of quasistable lattice defects by electronic excitation in SiO_2, Phys. Rev. Lett. 51 (1983) 423.
[187] K. Tanimura, L.E. Halliburton, Polarization of the X-ray-induced blue luminescence in quartz, Phys. Rev. B 34 (1986) 2933.
[188] C Itoh, et al., Optical studies of self-trapped excitons in SiO_2, J. Phys. C Solid State Phys. 21 (1988) 4693.
[189] W. Joosen, S. Guizard, P. Martin, G. Petite, P. Agostini, Femtosecond multiphoton generation of the self trapped exciton in α SiO_2, Appl. Phys. Lett. 61 (1992) 2260.
[190] K. Kajihara, L. Skuja, H. Hosono, Diffusion and reactions of photoinduced interstitial oxygen atoms in amorphous SiO_2 impregnated with 18O-labeled interstitial oxygen molecules, J. Phys. Chem. C 118 (2014) 4282.
[191] L. Skuja, M. Hirano, H. Hosono, Oxygen-related intrinsic defects in glassy SiO_2: interstitial ozone molecules, Phys. Rev. Lett. 84 (2000) 302.
[192] W. Heitmann, H.U. Bonewitz, A. Mühlich, New absorption bands in pure and F-doped silica optical fibres, IEE Electr. Lett. 19 (1983) 616.
[193] Claude Schweitzer, Reinhard Schmidt, Physical mechanisms of generation and deactivation of singlet oxygen, Chem. Rev. 103 (2003) 1685.
[194] L. Skuja, B. Güttler, D. Schiel, A.R. Silin, Quantitative analysis of the concentration of interstitial O_2 molecules in SiO_2 glass using luminescence and Raman spectrometry, J. Appl. Phys. 83 (1998) 6106.
[195] S. Agnello, L. Vaccaro, M. Cannas, K. Kajihara, Temperature dependence of O_2 singlet photoluminescence in silica nanoparticles, J. Non-Cryst. Solids 379 (2013) 220.
[196] S. Agnello, et al., Interstitial O_2 distribution in amorphous SiO_2 nanoparticles determined by Raman and Photoluminescence spectroscopy, J. Appl. Phys. 114 (2013) 104305.
[197] K. Kajihara, M. Hirano, Interstitial oxygen molecules in amorphous SiO_2. I. Quantitative concentration analysis by thermal desorption, infrared photoluminescence, and vacuum-ultraviolet optical absorption, J. Appl. Phys. 98 (2005) 013527.
[198] S. Agnello, et al., Near-infrared emission of O_2 embedded in amorphous SiO_2 nanoparticles, J. Phys. Chem. C 115 (2011) 12831.
[199] D.L. Griscom, Trapped-electron centers in pure and doped glassy silica: a review and synthesis, J. Non Cryst. Solids 357 (2011) 1945.
[200] D.L. Griscom, E.J. Friebele, S.P. Mukherjee, Studies of radiation-induced point defects in silica aerogel monoliths, Cryst. Latt. Def. Amorph. Mat. 17 (1987) 157.
[201] A. Alessi, S. Agnello, F.M. Gelardi, Properties and generation by irradiation of germanium point defects in Ge-doped silica, Germanium: Properties, Production and Applications, Nova Science Publishers, Hauppauge, NY, USA, 2012, pp. 75–150 ISBN:978-1-61209-205-8.
[202] J. Bisutti, Etude De La Transmission Du Signal Sous Irradiation Transitoire Dans Les Fibres Optiques, Thèse de Doctorat, Université de Saint-Etienne, Saint-Etienne, France, 2010.
[203] D. Di Francesca, et al., X-ray irradiation effects on fluorine-doped germanosilicate optical fibers, Opt. Mater. Express 4 (2014) 1683.
[204] G. Origlio, Properties and Radiation Response of Optical Fibers: Role of Dopants, Université de Saint-Etienne, France, 2009 PhD Thesis.
[205] S. Girard, J. Baggio, J. Bisutti, 14-MeV neutron, gamma-ray, and pulsed X-ray radiation-induced effects on multimode silica-based optical fibers, IEEE Trans. Nucl. Sci. 53 (2006) 3750.
[206] V.B. Neustruev, Color centres in germanosilicate glass and optical fibres, J. Phys. Condens. Mater. 6 (1994) 6901.
[207] D.L. Griscom, Gamma-ray-induced optical attenuation in Ge-doped-silica fiber image guides, J. Appl. Phys.78(1995) 6697.
[208] E.V. Anoikin, V.M. Mashinski, V.B. Neustruev, Y.S. Sidorin, Effects of exposure to photon of various energies on transmission of germanosilicate optical fiber in the visible to near IR spectral range, J. Non-Cryst. Solids 179 (1994) 243.
[209] K. Awazu, H. Kawazoe, M. Yamane, Simultaneous generation of optical absorption bands 5.14 and 0.452 eV in 9 SiO_2:GeO_2 glasses heated under H_2 atmosphere, J. Appl. Phys. 68 (1990) 2713.
[210] M. Fujimaki, et al., Structural changes induced by KrF excimer laser photons in H_2-loaded Ge-doped SiO_2 glass, Phys. Rev. B 60 (7) (1999) 4682–4687.
[211] N. Chiodini, et al., Optical transitions of paramagnetic Ge sites created by X-ray irradiation of oxygen-defect-free Ge-doped SiO_2 by the sol-gel method, Phys. Rev. B 60 (1999) 2429.
[212] E.V. Anoikin, et al., Formation and bleaching of colour centres in germanium-doped silica glass by 3.68 eV photons, Sov. Lightw. Commun. 1 (1991) 29.
[213] Luigi Giacomazzi, et al., Ge(2), Ge(1) and Ge-E' centers in irradiated Ge-doped silica: a first-principles EPR study, Opt. Mater. Express 5 (2015) 1054.
[214] L. Skuja, A. Naber, Site-selective luminescence study of defects in gamma-irradiated glassy germanium dioxide, Nucl. Instrum. Methods B 116 (1996) 549.
[215] M. Cannas, G. Origlio, Ultraviolet optical properties of silica controlled by hydrogen trapping at Ge-related defects, Phys. Rev. B 75 (2007) 233201.
[216] K. Awazu, K.-I. Muta, H. Kawazoe, Formation mechanism of hydrogen-associated defect with an 11.9mT doublet in electron spin resonance and red luminescence in SiO_2:GeO_2 fibers, J. Appl. Phys. 74 (1993) 2237.
[217] D.P. Poulios, J.P. Spoonhower, N.P. Bigelow, Influence of oxygen deficiencies and hydrogen-loading on defect luminescence in irradiated Ge-doped silica glasses, J. Lumin. 101 (2003) 23.
[218] A. Alessi, et al., Evidence of different red emissions in irradiated germanosilicate materials, J. Lumin. 177 (2016) 127.
[219] P F Kashaykin, et al., New radiation colour centre in germanosilicate glass fibres, Quant. Electron. 48 (2018) 1143.
[220] D.L. Griscom, E.J. Friebele, K.J. Long, J.W. Fleming, Fundamental defect centers in glass: electron spin resonance and optical absorption studies of irradiated phosphorus-doped silica glass and optical fibers, J. Appl. Phys. 54 (1983) 3743.
[221] G.M. Ermolaeva, et al., Low-dispersion optical fiber highly transparent in the UV spectral range, Opt. Eng. 43 (2004) 2896.
[222] E.J. Friebele, D.L. Griscom, Color center in glass optical fiber waveguides, Mat. Res. Soc. Symp. Proc. 61 (1986) 319.
[223] H. Hosono, K. Kajihara, M. Hirano, Photochemistry in phosphorus-doped silica glass by ArF excimer laser irradiation: Crucial effect of H2 loading, *J. Appl. Phys.* **91** (2002) 4121.
[224] L. Giacomazzi, et al., Optical absorption spectra of P defects in vitreous silica, Opt. Mat. Express 8 (2018) 385.

[225] A.A. Rybaltovsky, et al., Photoinduced absorption and refractive-index induction in phosphosilicate fibres by radiation at 193 nm, Quant. Electron. 37 (2007) 388.

[226] G. Origlio, et al., Optical properties of phosphorus-related point defects in silica fiber preforms, Phys. Rev. B 80 (2009) 205208.

[227] M. Engholm, P. Jelger, F. Laurell, L. Norin, Improved photodarkening resistivity in ytterbium-doped fiber lasers by cerium codoping, Opt. Lett. 34 (2009) 1285.

[228] A.N. Trukin, et al., Photosensitivity of SiO$_2$–Al and SiO$_2$–Na glasses under ArF (193 nm) laser, J. Non-Cryst. Solids 355 (2009) 1066.

[229] J.C. Lagomacini, et al., Growth kinetics of AlOHC defects in γ-irradiated silica glasses, J. Non-Cryst. Solids 403 (2014) 5.

[230] A. Alessi, et al., Radiation effects on aluminosilicate optical fibers: spectral investigations from the ultraviolet to near-infrared domains, Phys. Status Solidi A (2018) 1800485.

[231] A.V. Faustov, et al., Comparison of gamma-radiation induced attenuation in Al-doped, P-doped and Ge-doped fibres for dosimetry, IEEE Trans. Nucl. Sci. 60 (2013) 2511.

[232] H. Hosono, H. Kawazoe, Radiation-induced coloring and paramagnetic centers in synthetic SiO$_2$:al glasses, Nucl. Instrum. Methods Phys. Res. B 91 (1994) 395.

[233] A.S. Zyubin, A.M. Mebel, S.H. Lin, Quantum chemical modeling of photoabsorption and photoluminescence of the [AlO4]0 defect in bulk SiO$_2$, J. Chem. Phys. 119 (2003) 11408.